



RESEARCH

Open Access



NLRP3 inflammasome-mediated choroid plexus hypersecretion contributes to hydrocephalus after intraventricular hemorrhage via phosphorylated NKCC1 channels

Zhaoqi Zhang^{1,2,3}, Qiang Tan^{1,2,3}, Peiwen Guo^{1,2,3}, Suna Huang^{1,2,3}, Zhengcai Jia^{1,2,3}, Xin Liu^{1,2,3}, Hua Feng^{1,2,3*}  and Yujie Chen^{1,2,3,4*} 

Abstract

Background: Hydrocephalus is a severe complication of intracerebral hemorrhage with ventricular extension (ICH-IVH) and causes cerebrospinal fluid (CSF) accumulation. The choroid plexus epithelium plays an important role in CSF secretion and constitutes the blood–CSF barrier within the brain–immune system interface. Although the NLRP3 inflammasome, as a key component of the innate immune system, promotes neuroinflammation, its role in the pathogenesis of hydrocephalus after hemorrhage has not been investigated. Therefore, this study aimed to investigate the potential mechanism of NLRP3 in hydrocephalus to discover a potential marker for targeted therapy.

Methods: A rat model of hydrocephalus after ICH-IVH was developed through autologous blood infusion in wild-type and *Nlrp3*^{-/-} rats. By studying the features and processes of the model, we investigated the relationship between the NLRP3 inflammasome and CSF hypersecretion in the choroid plexus.

Results: The ICH-IVH model rats showed ventricular dilation accompanied by CSF hypersecretion for 3 days. Based on the choroid plexus RNA-seq and proteomics results, we found that an inflammatory response was activated. The NLRP3 inflammasome was investigated, and the expression levels of NLRP3 inflammasome components reached a peak at 3 days after ICH-IVH. Inhibition of NLRP3 by an MCC950 inflammasome inhibitor or *Nlrp3* knockout decreased CSF secretion and ventricular dilation and attenuated neurological deficits after ICH-IVH. The mechanism underlying the neuroprotective effects of NLRP3 inhibition involved decreased phosphorylation of NKCC1, which is a major protein that regulates CSF secretion by altering Na⁺- and K⁺-coupled water transport, via MCC950 or *Nlrp3* knockout. In combination with the in vitro experiments, this experiment confirmed the involvement of the NLRP3/p-NKCC1 pathway and Na⁺ and K⁺ flux.

*Correspondence: fenghua8888@vip.163.com; fenghua@tmmu.edu.cn; yujiechen6886@foxmail.com; chenyj@tmmu.edu.cn

¹ Department of Neurosurgery and State Key Laboratory of Trauma, Burn and Combined Injury, Southwest Hospital, Third Military Medical University (Army Medical University), 29 Gaotanyan Street, Shapingba District, Chongqing 400038, China

Full list of author information is available at the end of the article



© The Author(s) 2022. **Open Access** This article is licensed under a Creative Commons Attribution 4.0 International License, which permits use, sharing, adaptation, distribution and reproduction in any medium or format, as long as you give appropriate credit to the original author(s) and the source, provide a link to the Creative Commons licence, and indicate if changes were made. The images or other third party material in this article are included in the article's Creative Commons licence, unless indicated otherwise in a credit line to the material. If material is not included in the article's Creative Commons licence and your intended use is not permitted by statutory regulation or exceeds the permitted use, you will need to obtain permission directly from the copyright holder. To view a copy of this licence, visit <http://creativecommons.org/licenses/by/4.0/>. The Creative Commons Public Domain Dedication waiver (<http://creativecommons.org/publicdomain/zero/1.0/>) applies to the data made available in this article, unless otherwise stated in a credit line to the data.

Conclusions: This study demonstrates that NKCC1 phosphorylation in the choroid plexus epithelium promotes NLRP3 inflammasome-mediated CSF hypersecretion and that NLRP3 plays an important role in the pathogenesis of hydrocephalus after hemorrhage. These findings provide a new therapeutic strategy for treating hydrocephalus.

Keywords: Intraventricular hemorrhage, Hydrocephalus, NLRP3 inflammasome, Choroid plexus, NKCC1, Cerebrospinal fluid hypersecretion

Background

Intracerebral hemorrhage (ICH) occurs in 10–15% of all strokes worldwide each year [1]. Of the approximately 40% of ICH cases that develop intraventricular hemorrhage, 50% are complicated by hydrocephalus [2, 3]. Extension of the hemorrhage into the ventricular system after ICH leads to hydrocephalus, which is the accumulation of cerebrospinal fluid (CSF) in the ventricles [4]. Persistent elevations in intracranial pressure can cause acute brainstem herniation and, ultimately, death [5]. Invasive CSF shunting is the first line of treatment for hydrocephalus after hemorrhage, but it carries a high risk for serious complications, such as shunt obstruction or infection [6, 7]. Therefore, it is necessary to develop fast-acting, low-risk targeted pharmacotherapeutic strategies for treating patients with hydrocephalus [8].

CSF circulation failure is the major mechanism of hydrocephalus after hemorrhage. Most relevant studies have aimed to develop techniques for controlling the flow of CSF by targeting the obstruction. Hydrocephalus after hemorrhage becomes aggravated by damage to ependymal glia and dysfunction of arachnoid granulations, which can block the outflow of CSF [9, 10]. The Toll-like receptor 4 (TLR4) protein-dependent inflammatory response contributes to hydrocephalus by inducing hypersecretion of CSF [11]. CSF is predominantly produced by the choroid plexus, which is an epithelial monolayer that serves as the main component of the blood–CSF barrier [12, 13]. The $\text{Na}^+/\text{K}^+/\text{2Cl}^-$ cotransporter (NKCC1), which is expressed in the luminal membrane of the choroid plexus, contributes to approximately half of the production of CSF [14]. NKCC1 contributed to CSF formation by transporting Na^+ , K^+ , and Cl^- transmembrane coupled water, which permits water to be transported independently of, and even against, an osmotic gradient [15]. As a chloride importer antagonist of NKCC1, bumetanide attenuates many neurological and psychiatric disorders [16]. Intracerebroventricular injection of blood metabolites caused choroid plexus inflammation and hydrocephalus, but the mechanisms remain unclear. Secretory epithelia respond to proinflammatory stimulation by increasing the fluid secretion rate.

As a critical function of the innate immune response to tissue injury, the NLRP3 inflammasome is increasingly being considered to be a driver of injury after

hemorrhage; this inflammasome senses cellular deviation from homeostasis as a danger signal and subsequently initiates inflammatory responses [17–19]. The NLRP3 inflammasome releases cytokines (IL-1 β and IL-18) and exacerbates brain edema, disruption of the blood–CSF barrier, and neuronal apoptosis after ICH [20, 21]. Furthermore, when NLRP3 was suppressed (MCC950 or *Nlrp3*^{-/-}), the secondary brain injury caused by ICH was alleviated, and most relevant studies have aimed to investigate the NLRP3 inflammasome in immune cells, such as microglia, macrophages and astrocytes [22, 23]. However, no functional or regulatory interactions have been demonstrated in choroid plexus epithelial cells to date.

Despite partial elucidation of the underlying mechanism of hydrocephalus after hemorrhage, its pathogenesis is not well understood. To achieve a comprehensive understanding of the biological processes of this difficult-to-treat condition, based on transcriptomics and proteomics of the choroid plexus, we hypothesized that NLRP3 would aggravate hydrocephalus after ICH with ventricular extension (ICH-IVH) by altering NKCC1 phosphorylation to enhance CSF secretion in the choroid plexus. The present study investigated the function and molecular mechanism of the NLRP3 inflammasome in the pathogenesis of hydrocephalus with the aim of discovering a new therapeutic target for hydrocephalus patients.

Methods

Animals

Adult male Sprague-Dawley rats (220–250 g) were purchased from the Animal Experimental Center of Third Military Medical University (Chongqing, China). *Nlrp3*^{-/-} rats were purchased from Cyagen Biosciences (Guangzhou, China). The rats were housed in a temperature-controlled room under specific pathogen-free conditions and a standard 12-h light/dark cycle, with ad libitum access to food and water. All experimental procedures involving animals were performed in compliance with the Guidelines for the Care and Use of Laboratory Animals, approved by the Laboratory Animal Welfare and Ethics Committee of Third Military Medical University (AMUWEC2020762), and reported according to the ARRIVE (Animal Research: Reporting of In Vivo Experiments) guideline.

ICH-IVH and IVH models of hydrocephalus and drug treatment

The surgical procedures used in this study for rats subjected to hemorrhage followed the procedures that are described in detail in our previous study [9, 24]. In brief, the animals were anesthetized with pentobarbital (40 mg/kg, intraperitoneally). The right femoral artery was catheterized as the source for obtaining a blood sample. For the ICH-IVH model, the rats were positioned in a stereotaxic frame, in which a cranial burr hole (1 mm) was drilled (coordinates: 0.2 mm posterior and 2.2 mm lateral to bregma). A 29-gauge needle was inserted at a rate of 1 mm/min at a depth of 5.0 mm from the dura. Using a microinjection pump, 200 μ l of nonheparinized arterial blood was infused through the hole into the right caudate nucleus at a rate of 14 μ l/min. In the IVH model, only the location of the drilled hole, which was drilled at 0.6 mm posterior and 2.2 mm lateral to the bregma, was different from that in the ICH-IVH model, and the depth of the inserted needle was 4.5 mm. After ICH-IVH, all rats were randomly divided into 4 groups as follows: ICH-IVH, ICH-IVH + MCC950, ICH-IVH + MCC950 + MSU, and ICH-IVH + bumetanide (Fig. 1). The process of randomization was as follows: all ICH-IVH rats were numbered and separated into four groups according to automatic random number blind grouping. The NLRP3 inhibitor MCC950 (MCE, USA) dissolved in saline was administered at a dose of 10 mg/kg by intraperitoneal injection 1 h after ICH-IVH induction. The NLRP3 activator monosodium urate (Abcam, USA), dissolved in saline, was administered by intraperitoneal injection after the MCC950 injection. Bumetanide (MCE, USA) dissolved in saline was administered at a dose of 10 mg/kg by intraperitoneal injection each day after ICH-IVH induction. The ICH-IVH group was given an equal volume of normal saline at the same time. The sham group received only needle injections following the ICH-IVH rats.

Neurobehavioral examination

Modified Neurological Severity Score (mNSS)

The rats were evaluated for neurological dysfunction using the mNSS method, as described previously [25]. The mNSS is the result of a composite test of motor, sensory and balance functions. Briefly, the assessment was performed at 3 days and 7 days after ICH-IVH. Neurological function was graded on a scale of 0–18 (a score of 13–18 indicates severe injury, 7–12 indicates moderate injury, and 1–6 indicates mild injury).

Rotating beam test

A rotarod test was performed to evaluate sensorimotor deficits as previously described [26]. Briefly, animals

were placed on a rotarod cylinder (RWD, China). The time until the animals fell off the rotating cylinder was recorded.

Grip front test

The grip strength of the front limbs was measured by a grip strength meter (Laboratory Enterprises, Nasik, India), which consisted of a steel wire grid connected to an isometric force transducer following a method described earlier [27]. Each rat was measured in triplicate, and the average handgrip strength of each was recorded. The rats were gently pulled back when they grasped the grid with their forepaws until they released the grid, and the maximal force in Newtons exerted by the rats before they lost their grip was measured.

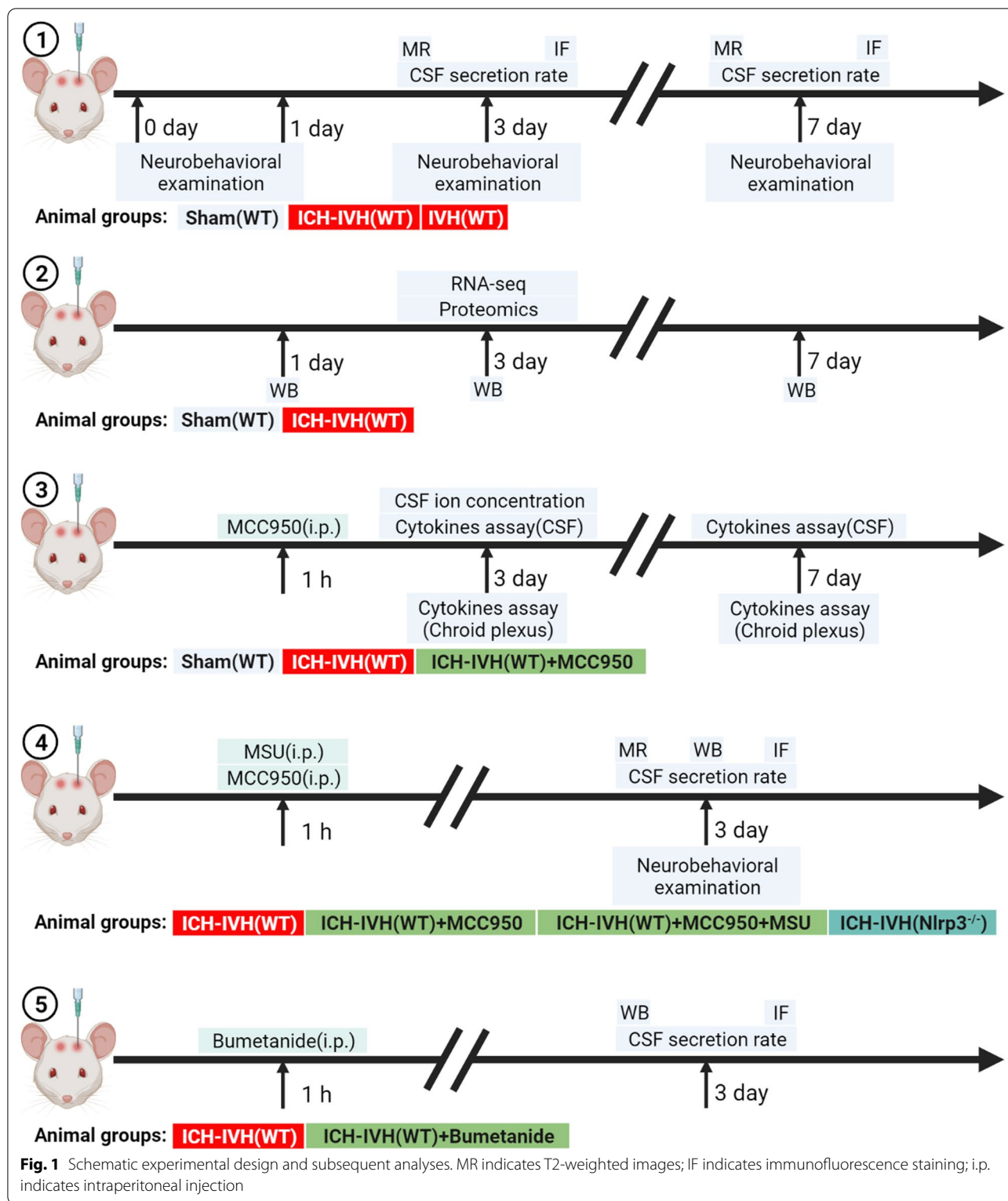
All behavioral tests were performed by an investigator who was blinded to the treatments.

Quantification of the CSF secretion rate

The rates of CSF production were measured using a method as previously described [28]. Briefly, anesthetized rats were mounted on a stereotaxic apparatus, and a cranial burr hole (1.2 mm) was drilled over the left lateral ventricle (coordinates relative to bregma: x , -0.6 cm; y , -1.6 cm). Next, the rat's head was rotated on the ear bars by 90° so that it was oriented nose down, and the suboccipital muscles were dissected to the cisterna magna to expose the atlantooccipital ligament. The ligament was punctured, and a 29-gauge needle was advanced 5 mm through the foramen of Magendie to the fourth ventricle. Sterile molecular-grade oil (100 μ l; Sigma-Aldrich) was infused through the tube to occlude the aqueduct of Sylvius, thereby creating a closed system of CSF circulation in the lateral ventricle. With the rat in the same position, a glass capillary tube (OD, 1.1 mm; ID, 1.0 mm; length, 20 cm) was advanced through the burr hole into the lateral ventricle (depth 4.5 mm ventral). The volume of CSF collected at a given time (20 min) was calculated as V (mm^3) = $\pi \cdot r^2 \cdot d$, where r is the radius of the glass capillary tube and d is the distance that CSF traveled within the capillary tube. The rate of CSF formation (μ l/min) was then calculated from the slope of the volume–time relationship.

Western blot analysis

Western blot analysis was performed as previously described [29]. The brains were perfused with saline before decapitation at day 3 post-injection. The choroid plexus tissue was sampled. The following primary antibodies were used: rabbit anti-NLRP3 (1:1000 dilution, Abcam, ab210491, UK); mouse anti-Caspase-1 (1:1000 dilution, Novus, 56565SS, USA); rabbit anti-IL-1 β (1:1000 dilution, Gene-Tex, 55675, USA); rabbit anti-p-NKCC1



(1:1000 dilution, Sigma-Aldrich, ABS1004, USA); rabbit anti-NKCC1 (1:1000 dilution, CST, 14581S, USA) and rabbit anti- β -actin (1:1000 dilution, CST, 8457, USA). The relative densities of the immunoreactive bands were

normalized to that of β -actin and then analyzed using ImageJ (National Institutes of Health, Bethesda, Maryland, USA).

Cytokine assay kits

Rats were anesthetized with pentobarbital (40 mg/kg intraperitoneal). CSF was collected through the cisterna magna; then, the rats were decapitated to obtain the choroid plexus. The CSF was centrifuged at 10,000 rpm to separate the supernatant. The choroid plexus was homogenized in ice-cold phosphate-buffered saline with protease inhibitor cocktails (Sigma-Aldrich, USA). Total protein concentration was quantified using a bicinchoninic acid protein assay (Boster, China). The CSF and choroid plexus cytokine levels were measured using inflammation cytokine assay kits (RayBiotech, USA) according to the manufacturer's instructions.

Immunofluorescence staining

Immunofluorescence staining of the brain tissue was performed on fixed frozen sections, as previously described [30]. Rats were anesthetized with pentobarbital (40 mg/kg intraperitoneal) and perfused with 4% paraformaldehyde after deep anesthesia was achieved. The brain was isolated, and then the choroid plexus was dissected under magnification using sharp forceps. The choroid plexus was subsequently immersed in 30% sucrose for 3–4 days at 4 °C. The tissues were embedded in an optimal cutting temperature compound (Sakura, USA), and 12-mm-thick slices were cut using a cryostat. The slices were incubated with the following primary antibodies at 4 °C overnight: a rabbit antibody to NLRP3 (1:200 dilution, ab4207, Abcam, UK), a rabbit antibody to laminin (1:100 dilution, Abcam, UK), a rabbit antibody to AE2 (1:200 dilution, ab42687, Abcam, UK), a goat antibody to NLRP3 (1:100, Gene-Tex, USA), a rabbit antibody to AE2 (1:200 dilution, Abcam, UK) and a rabbit antibody to p-NKCC1 (1:200 dilution, ABS1004, Sigma-Aldrich, USA). Then, the slices were probed with appropriate secondary antibodies for 2 h at 37 °C. Finally, the slices were counterstained with 4',6-diamidino-2-phenylindole (Boster, China) and examined using a confocal fluorescence microscope (LSM780, Zeiss).

Cell counts

Cells were counted 3 days after ICH-IVH. For quantification of the positive cells in the choroid plexus, consecutive slices were made in two sections per animal ($n=6$ per group), with a 40- μ m space in between used for cell counts. Three high-power images were used for cell counting. NLRP3- and p-NKCC1-positive cells were counted in the choroid plexus. Cell counts were performed by two researchers in a blinded manner. All measurements were repeated three times, and the mean values were used.

MRI and ventricular volume analysis

Rats were anesthetized with a 2% isoflurane/air mixture throughout MRI examination. The MRI scans were performed using a 7.0-T Varian MR scanner (Bruker, USA) with a T2*gradient-echo sequence and a T2 fast spin-echo sequence using a view field of 35 mm \times 35 mm and 17 coronal slices (1.0 mm thickness). There are two classical methods for evaluating hydrocephalus based on MRI, i.e., the Evans index and whole-ventricle volume assessments [31]. Considering the time window and goals of our experiments, the whole-ventricle volume was calculated as according to a previously described method [32]. Bilateral ventricles and the hippocampus were outlined, and the areas of all slices were multiplied by the section thickness [33]. The 3D reconstruction of ventricular systems was based on the 3D Slicer. All image analyses were performed using ImageJ (National Institutes of Health, Bethesda, Maryland, USA) by two observers in a blinded manner.

CSF collection and metal detection

CSF was collected by inserting a syringe into the cisterna magna, and the collected CSF was centrifuged at 10,000 $\times g$ for 5 min at 4 °C to remove any tissue debris. Inductively coupled plasma-optical emission spectrometry (ICP-OES) was used for K⁺ and Na⁺ quantification. All tests were performed with 5–10 μ l of CSF.

Transcriptome sequencing, quantitative proteomic and integrated analysis

Quantitative RNA sequencing

The rats in the sham group and ICH-IVH group (3 days) were anaesthetized on ice and dissected longitudinally to obtain the choroid plexus ($n=6$ in each group, 3 replicates). Total RNA of the choroid plexus was isolated using TRIzol reagent (Invitrogen, USA). The quantity and purity of total RNA were then detected by a NanoDrop ND-1000 instrument (NanoDrop, USA). Furthermore, RNA integrity was detected by an Agilent 2100 instrument, and a RIN > 7.0 was taken as the qualified standard. Then, the qualified RNA was provided to LC-Bio Technology Co., Ltd. (Hangzhou city, China), for subsequent library preparation and sequencing using a HiSeq 4000 platform as described previously [34]. The expression levels of all transcripts were then evaluated by calculating the fragments per kilobase per million reads (FPKM). The thresholds of significantly different expression were $p < 0.05$ and FPKM > 1. The GO and KEGG databases were used to explore the functions and biological pathways in which the differentially expressed genes were involved.

Proteomics analysis

The choroid plexus was rapidly frozen and ground in liquid nitrogen and then treated as previously reported to obtain the purified protein concentration [35]. Briefly, TMT reagent (Thermo Fisher Scientific) was added to the prepared protein suspension to obtain a peptide mixture for sequencing by LC-Bio (<http://www.lc-bio.com/>). Differentially expressed proteins were defined as proteins with a fold-change greater than 1.2 and a p value (t -test) less than 0.05. Functional classification of differentially expressed proteins was conducted by mapping with GO terms, and the highest bit score sequence was selected. Pathway analysis was performed using the KEGG database.

Primary choroid plexus epithelial cell cultures and stimulator administration

Primary choroid plexus epithelial cells from rats were cultured as previously described [36]. In brief, the brains of P14 rats were isolated, and the choroid plexus was isolated and plated into freshly prepared sterile dissection media. Dissection media included $1 \times$ DPBS with 0.6% glucose and $1 \times$ Pen-Strep. The tissue was then resuspended in a working solution (a mixture of $5 \times$ collagenase [type II] and $1 \times$ HBSS supplemented with 3 mM CaCl_2 at a 1:5 ratio) and incubated at 37 °C for 20 min; the tubes were tapped every 5 min. CPEC media included 10% FBS and 10,000 units/ml Pen-Strep in DMEM. Tissue was dissociated using a pipette and then plated on poly-D-lysine and laminin-coated cell culture plasticware. Choroid plexus epithelial cells were cultured for 14 days, with the media changed every 2–3 days, and then used for experiments. Cells were treated with 1 $\mu\text{g}/\text{ml}$ LPS or 1 $\mu\text{g}/\text{ml}$ lysis-RBCs for 12 h. Thirty minutes after incubation with lysis-RBCs, MCC950 (5 μM) was added.

Statistical analysis

The data were analyzed and plotted by GraphPad Prism and presented as the means \pm SEMs. Sample sizes were calculated using an a priori sample size calculator with the following assumptions: $\alpha = 0.05$; two-tailed; and desired power, 80%. The results indicated that a minimum of 3 rats per group were needed. All data were analyzed using GraphPad Prism and satisfied a normal

distribution and the homogeneity of variance. Immunostaining, cytokine measurement data, and behavioral experiments were subjected to one-way ANOVA. Student's t -test was used for single comparisons, and analysis of variance with post hoc Bonferroni–Dunn correction was used for multiple comparisons, depending on the experiments. A p value < 0.05 was considered to be statistically significant. The number of different experimental groups and statistical methods is shown in the figure legends, and statistical analysis data are detailed in the Additional file 1: Statistical results.

Results

ICH-IVH induced CSF hypersecretion and hydrocephalus and neurocognitive functional deficits

According to a previous posthemorrhagic hydrocephalus animal model, intraventricular hemorrhage (IVH) and ICH-IVH rat models were constructed [9]. Both of them obviously involved hydrocephalus. We first evaluated the degree of hydrocephalus in the two different rat models by measuring lateral ventricular volumes according to T2 magnetic resonance imaging (MRI) scans combined with 3D reconstruction images at 3 and 7 days after hemorrhage (Fig. 2A). We found that ICH-IVH had more obvious lateral ventricular dilation than did IVH. Both of them already showed severe hydrocephalus 3 days after hemorrhage and worsened over time. Compared with the sham group, both hemorrhage groups had more obvious lateral ventricular volumes, which indicated hydrocephalus (Fig. 2B). The occurrence of hydrocephalus depends on CSF circulation failure, which involves two main aspects: CSF formation and outflow [37]. Laminin staining of arachnoid granules was performed to investigate whether the flowing-out deficits occurred at 3 days after hemorrhage. The images showed that there was no arachnoid granule fibrosis to influence the CSF outflow and contribute to hydrocephalus until 7 days after hemorrhage (Fig. 2D). Therefore, we speculated that more CSF produced by the choroid plexus mediated hydrocephalus during the acute phase of 3 days. Based on previous methods [28], we measured the CSF secretion rate in vivo and found that the CSF secretion rate was elevated after hemorrhage. Additionally, the ICH-IVH group had a higher CSF secretion rate than the IVH group did at

(See figure on next page.)

Fig. 2 CSF secretion rate and hydrocephalus evaluation index after ICH-IVH and IVH. **A** Representative T2-weighted images and 3D reconstruction of lateral ventricles obtained on day 3 and day 7 in the IVH and ICH-IVH groups. **B** Quantification volumes of the lateral ventricle according to the related T2-weighted images (6 rats/group, one-way ANOVA). **C** Quantification of CSF secretion rates in sham, IVH and ICH-IVH rats at 3 and 7 days (6–8 rats/group, one-way ANOVA). **D** Representative images of immunofluorescence staining for laminin expression in arachnoid granules. Bar = 50 μm . **E** Number of hindlimb drops recorded for a walking task in which the rat walks over a rotating beam toward the home cage on a platform (6 rats/group, one-way ANOVA). **F** Testing for front grip strength at different time points (6 rats/group, one-way ANOVA). **G** mNSS (6 rats/group, one-way ANOVA). The results are presented as the means \pm SDs; ** $p < 0.01$ and * $p < 0.05$: sham group versus ICH-IVH group. # $p < 0.05$: sham group versus IVH group

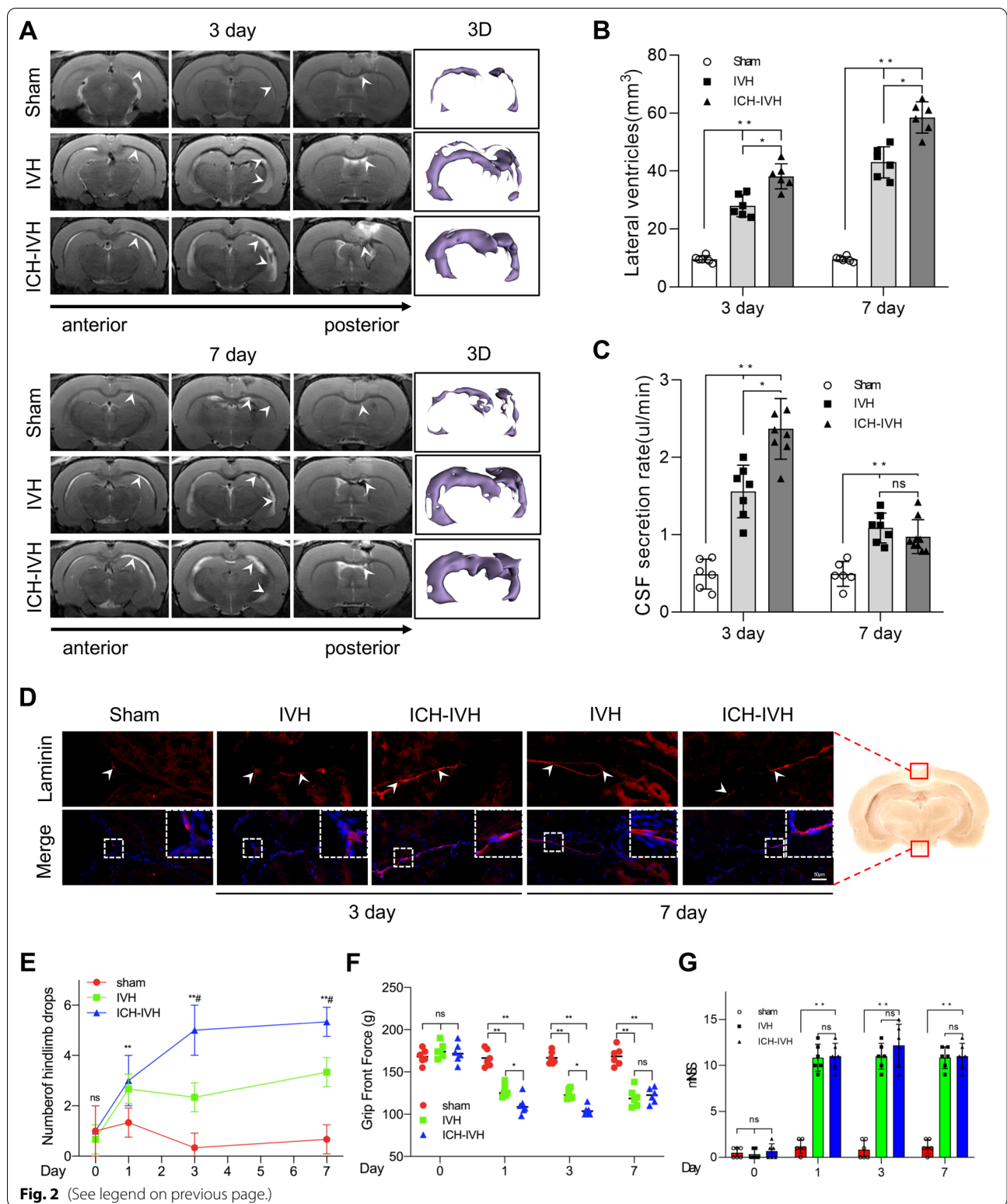


Fig. 2 (See legend on previous page.)

both 3 days and 7 days. In addition, the CSF secretion rate decreased over time after hemorrhage and reached a peak at 3 days (Fig. 2C). To determine whether the high

CSF secretion rate mediated acute-phase hydrocephalus and influenced the neurofunctions, we assessed the neurofunctions after hemorrhage. Hindlimb tests were

used to evaluate the balance ability. We compared the number of hindlimb drops after hemorrhage and found that the hemorrhage groups experienced similar deficits, especially the ICH-IVH group (Fig. 2E). Next, we tested the grip front force and found that the grip front force weakened in the hemorrhage groups (Fig. 2F). The mNSS comprehensively evaluated neurofunctions and showed that the hemorrhage groups had severe neurological deficits (Fig. 2G). According to the neurofunction tests, we found hydrocephalus after hemorrhage in rats with neurodeficit. Thus, it can be concluded that the ICH-IVH group had more severe neurodeficit than the IVH group did. Taken together, these data confirmed that the ICH-IVH groups had obvious hydrocephalus and neurodeficit in the acute phase and that CSF secretion contributed to hydrocephalus in this phase.

Quantitative transcriptome sequencing and proteomic analysis of the choroid plexus revealed inflammatory protein and RNA accumulation after ICH-IVH

We dissected the brains of six pairs of sham and ICH-IVH rats to expose the choroid plexus and performed quantitative tandem mass spectrometry experiments using 10-plex tandem mass tag labeling. Transcriptome sequencing was performed on 32624 RNAs, and 938 RNAs were obviously changed after ICH-IVH. In total, we quantified 8490 proteins that overlapped in the two groups. Compared with the sham group, the ICH-IVH group had 1162 significantly changed proteins ($p < 0.05$). According to transcriptome and proteomic analysis of the choroid plexus, we found some change trends at the RNA and protein levels (Fig. 3A), indicating that our quantitative mass spectrometry method could differentiate the choroid plexus transcriptome and proteome by hemorrhage. A volcano map of transcriptome sequencing shows the significantly different genes, and the top 30 genes are marked, including some inflammation- and innate immunity-related genes (Fig. 3B). Proteomic analysis of the volcano map showed significantly different proteins, and we marked the top 30 obviously changed proteins (Fig. 3C). Furthermore, using GO enrichment and pathway enrichment to explore the functions of these genes, we found that the inflammatory response was obviously activated in the choroid plexus after hemorrhage (Fig. 3D,

E). According to genes whose expression obviously changed at the RNA level, we marked the top 30 inflammation-related genes in the heatmap (Fig. 3F). A combined heatmap of proteomic analysis marked the top 30 proteins related to inflammation (Fig. 3G). The NLRP3 inflammasome was selected from inflammation-related genes according to transcriptome and proteomic analysis for further investigation. The NLRP3 inflammasome plays an important role in the CNS and contributes to many kinds of biological processes, including immune and inflammatory responses, and is highly expressed in macrophages, microglia, astrocytes, and epithelial cells. Studies on the NLRP3 inflammasome in epithelial cells are rare, especially in terms of choroid plexus epithelial cells. Therefore, we investigated the function of NLRP3 in hydrocephalus.

Time course of NLRP3 inflammasome changes in the choroid plexus after ICH-IVH

On the basis of the results of the transcriptome and proteomic analysis, we aimed to explore NLRP3 function in the choroid plexus after ICH-IVH. The time course of NLRP3 protein expression showed that NLRP3 was upregulated in the choroid plexus after ICH-IVH and peaked at 3 days after ICH-IVH (Fig. 4A). Choroid plexus epithelial cells are the major component of the choroid plexus, which is located in the ventricle systems. Combined with AE2 (a specific protein marker of the choroid plexus) staining results, the choroid plexus was mainly located in the lateral ventricle, which was selected as a sample collection position (Fig. 4B). In addition, we found more NLRP3-positive cells in the choroid plexus after ICH-IVH than in the sham group (Fig. 4C). Western blots used for quantitative analysis showed that the NLRP3 inflammasome and related proteins, IL-1 β and caspase-1, were also upregulated after ICH-IVH (Fig. 5E–H). We also used assay kits to measure cytokines in the choroid plexus and CSF, and the reported NLRP3-related cytokines IL-1 and IL-18 presented higher levels in the ICH-IVH group than in the sham group (Fig. 6A, B). These results demonstrated that NLRP3 inflammasome components were activated in choroid plexus epithelial cells after ICH-IVH and peaked at 3 days.

(See figure on next page.)

Fig. 3 Transcriptome and proteomic sequencing was performed to explore inflammation pathways activated after ICH-IVH in the choroid plexus. **A** Venn diagram showing RNA and protein sequencing. **B** Volcano map showing significantly changed genes identified by transcriptome sequencing between the sham group and ICH-IVH group. **C** Volcano map showing significantly changed genes identified by proteomic sequencing after ICH-IVH. **D** GO enrichment of transcriptome sequencing showing that the inflammatory response was upregulated after ICH-IVH. **E** KEGG pathway enrichment of transcriptome sequencing showed that NOD-like receptors were upregulated after ICH-IVH. **F** Heatmap of transcriptome sequencing showing the top 30 genes related to inflammation between the sham group and ICH-IVH group. **G** Heatmap of proteomic sequencing showing the top 30 proteins related to inflammation after ICH-IVH

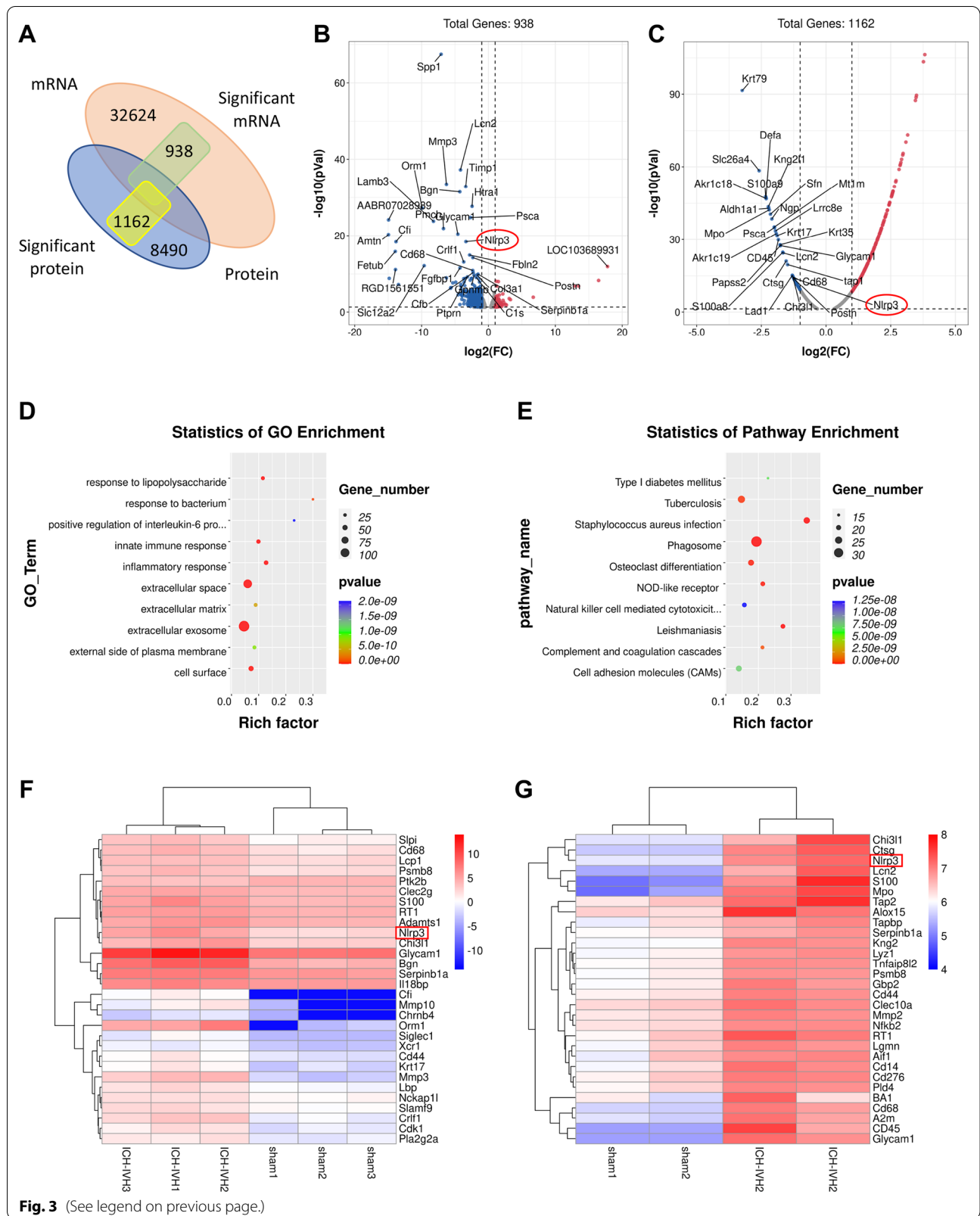


Fig. 3 (See legend on previous page.)

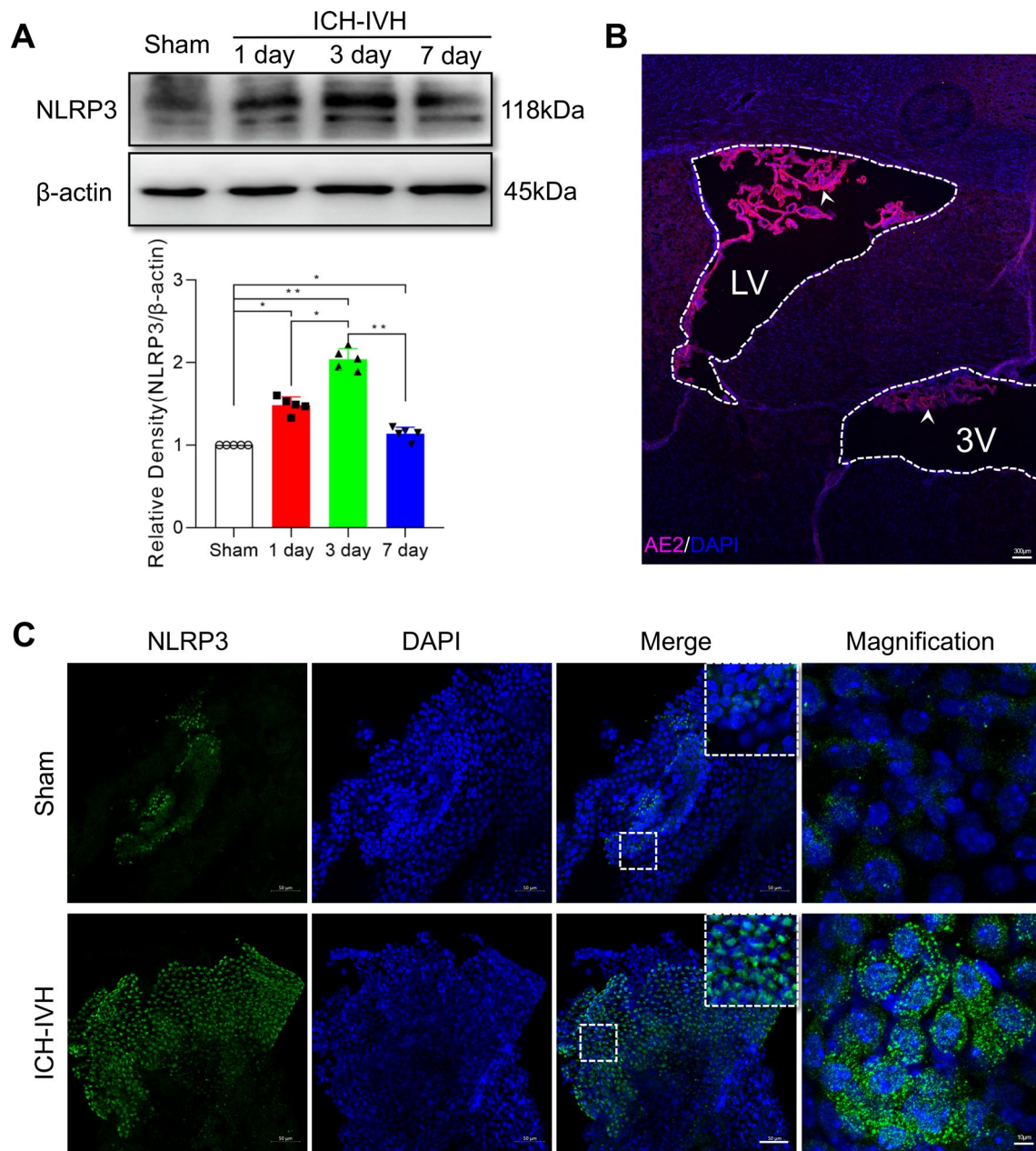


Fig. 4 NLRP3 inflammasome components were activated after ICH-IVH in the choroid plexus. **A** Western blot analysis of NLRP3 in the choroid plexus over time and statistical analysis of NLRP3 protein levels achieved at a maximum of 3 days after ICH-IVH ($n = 5, 6$ rats/sample, one-way ANOVA). **B** Representative images showing the choroid plexus AE2 location in ventricular systems; LV: lateral ventricle; 3V: the third ventricle; the white arrow indicates the choroid plexus. Bar = 300 μ m. **C** Representative fluorescence photomicrographs showing immunolabeling for NLRP3-positive cells in the choroid plexus 3 days after ICH-IVH (6 rats/group). Bar = 50 μ m. The values are expressed as the means \pm SDs; ** $p < 0.01$; * $p < 0.05$

Treatment with MCC950 or *Nlrp3*^{-/-} rats reduced CSF secretion, ameliorated hydrocephalus, and improved neurofunction

NLRP3 was selected as the main inflammation target in the acute-phase response and was upregulated in choroid

plexus epithelial cells, with a simultaneous increase in CSF secretion. To determine whether NLRP3 was a therapeutic target for adjusting CSF secretion for hydrocephalus in choroid plexus epithelial cells, MCC950 was first selected to inhibit NLRP3, a specific inhibitor

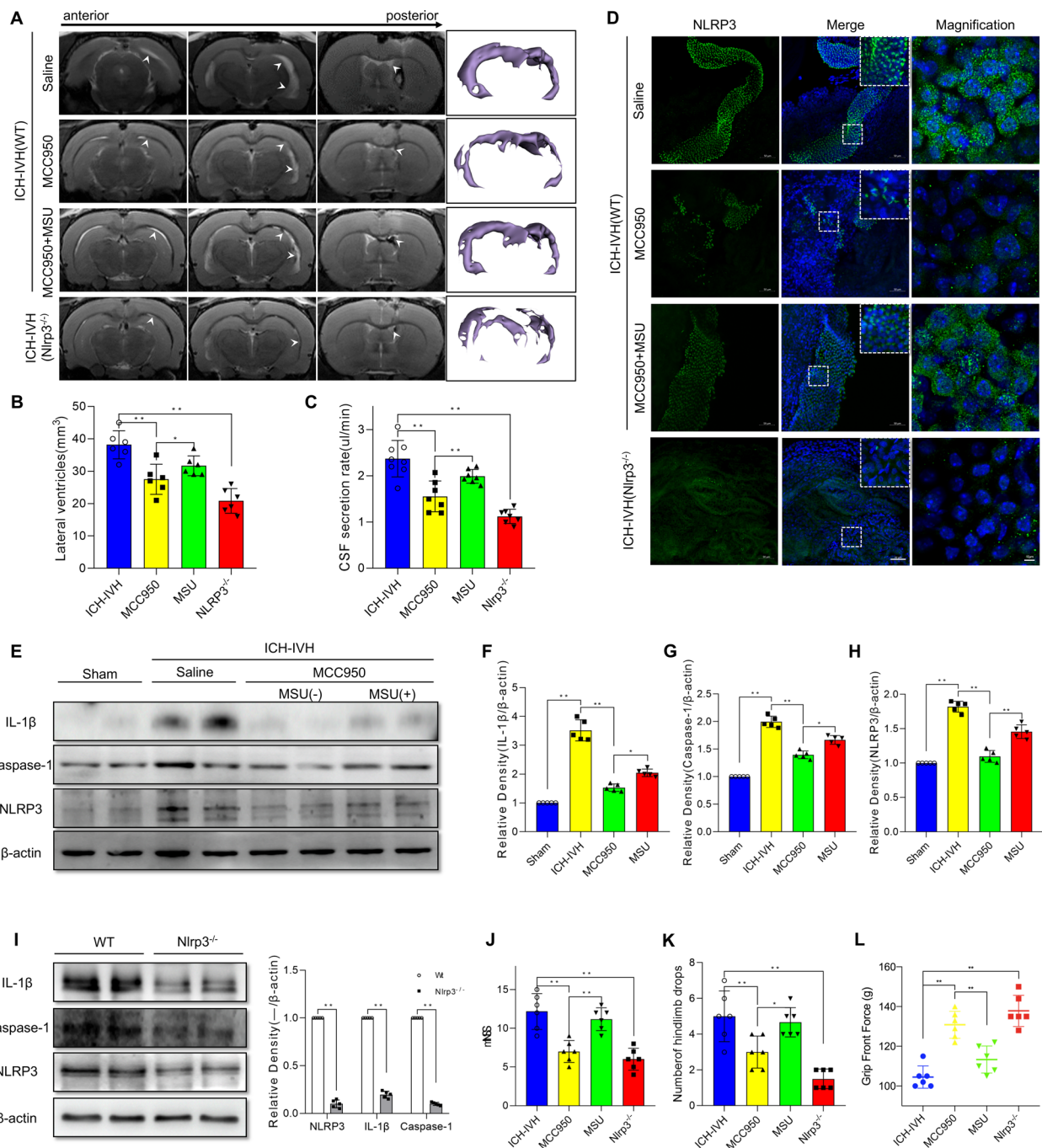
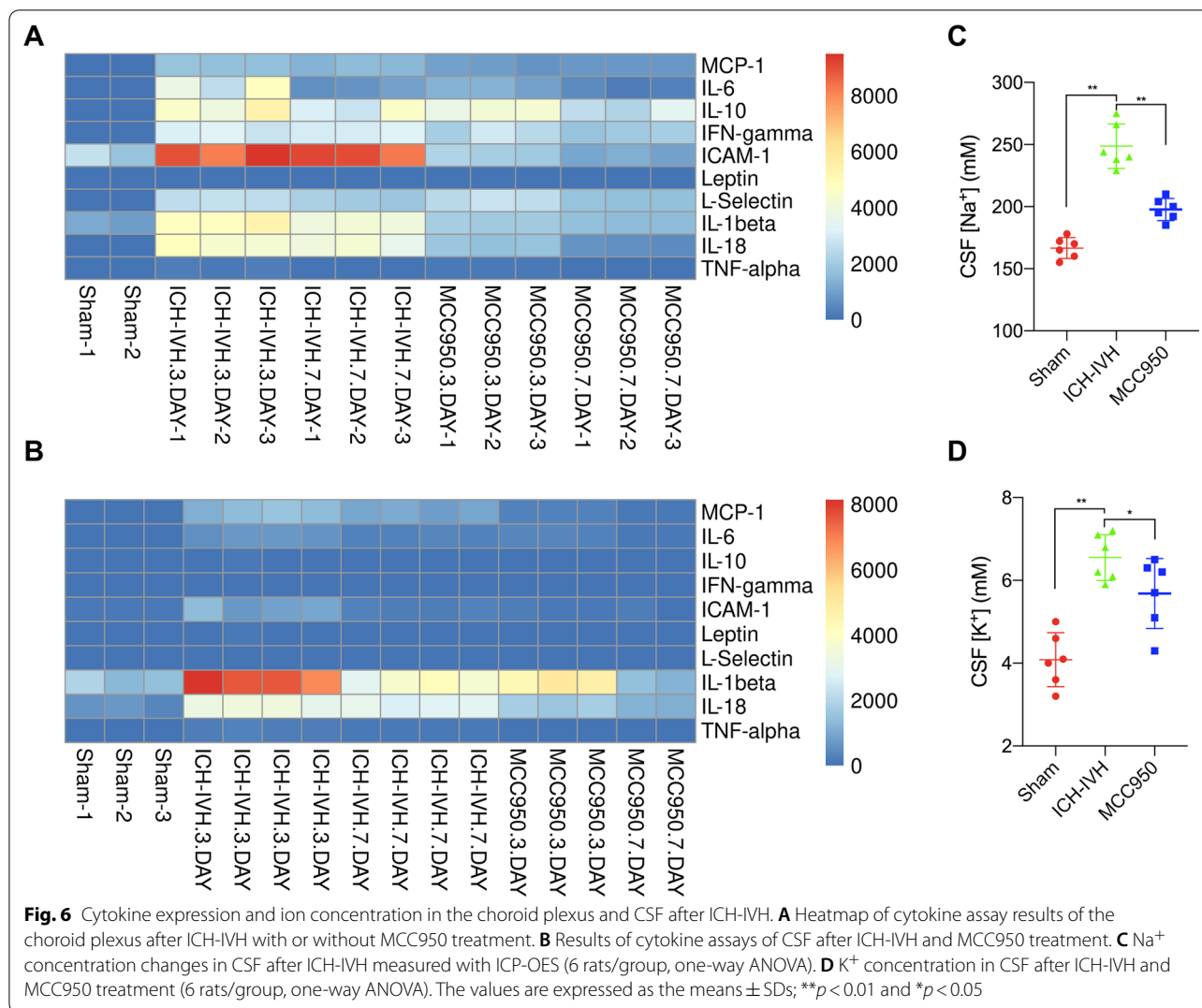


Fig. 5 Inhibitor or knockout of NLRP3 decreased NLRP3-related inflammation, CSF secretion and hydrocephalus. **A, B** Representative T2-weighted images of brain tissue, 3D reconstruction of the lateral ventricle after different NLRP3 treatments (**A**) and lateral ventricle volumes (**B**) measured via T2-weighted images (6 rats/group, one-way ANOVA). **C** CSF secretion rate in the MCC950-inhibited NLRP3 and *Nlrp3*^{-/-} groups (6–8 rats/group, one-way ANOVA). **D** Representative images of immunofluorescence staining for NLRP3 expression in the choroid plexus 3 days after ICH-IVH and different treatments. Bar = 50 μ m. **E–H** Western blot analysis of NLRP3, caspase-1, and IL-1 β in the choroid plexus of ICH-IVH rats, MCC950-treated rats and MSU-treated rats on day 3 ($n = 5$, 6 rats/sample, one-way ANOVA). **I** Western blot analysis of NLRP3, caspase-1, and IL-1 β in the choroid plexus of ICH-IVH in the control and *Nlrp3*^{-/-} groups ($n = 5$, 6 rats/sample, Welch’s two-tailed unpaired *t*-test). **J** mNSS (6 rats/group, one-way ANOVA). **K** Number of hindlimb drops recorded for a walking task in which the rat walks over a rotating beam toward the home cage on a platform (6 rats/group, one-way ANOVA). **L** Testing for front grip strength at different time points (6 rats/group, one-way ANOVA). **B, C, F–H, J–L** ICH-IVH indicates ICH-IVH (WT) + saline; MCC950 indicates ICH-IVH (WT) + MCC950; MSU indicates ICH-IVH (WT) + MCC950 + MSU; *Nlrp3*^{-/-} indicates ICH-IVH (*Nlrp3*^{-/-}). The values are expressed as the means \pm SDs; ** $p < 0.01$ and * $p < 0.05$



of NLRP3. The NLRP3 activator MSU was also used to explore NLRP3's function in hydrocephalus. In the ICH-IVH rats, MCC950 treatment decreased the lateral ventricle volumes and CSF secretion rates compared with those in the saline injection group (Fig. 5A–C). When NLRP3 was activated again by MSU after MCC950 was used to inhibit NLRP3, the MCC950 + MSU group had larger lateral ventricles and higher CSF secretion rate than the MCC950 group did after ICH-IVH (Fig. 5A–C). In total, the lateral ventricle volumes and CSF secretion rate changed as NLRP3 intervened. These results indicated that NLRP3 is related to CSF hypersecretion-mediated hydrocephalus. At the same time, we evaluated NLRP3-positive cells in the choroid plexus and found that NLRP3-positive cell counts had the same change trend as the CSF secretion rate and lateral ventricular volumes (Fig. 5D). Additionally, western blots were used to quantitatively analyze NLRP3 and related protein

expression. The results showed that NLRP3, IL-1 β , and Caspase-1 were downregulated after MCC950 treatment in ICH-IVH rats, and MSU treatment intervened in NLRP3-related protein levels in the choroid plexus (Fig. 5E–H). To further explore NLRP3's contribution to hydrocephalus, we developed *Nlrp3*^{-/-} rats and found that the *Nlrp3*^{-/-} group had lower CSF secretion and lateral ventricular volumes than the control group did after ICH-IVH (Fig. 5A–C). NLRP3 staining and quantitative analysis were used to evaluate NLRP3 expression levels, and NLRP3-positive cells were obviously decreased in the *Nlrp3*^{-/-} group (Fig. 5D). NLRP3, IL-1 β and Caspase-1 were also drastically reduced in the *Nlrp3*^{-/-} group compared with the control group after ICH-IVH (Fig. 5I). Neurofunction (mNSS, number of hindlimb drops, and grip front force) was assessed in different groups, and neurofunction improved in both the MCC950-treated group and the *Nlrp3*^{-/-} group after ICH-IVH compared

with the control (saline) group (Fig. 5J–L). In summary, these results indicated that NLRP3-mediated CSF hypersecretion plays an important role in the occurrence of hydrocephalus after ICH-IVH.

Inflammatory cytokines are upregulated in the choroid plexus and CSF after hemorrhage

It has been suggested that NLRP3 activation in the choroid plexus contributes to hydrocephalus by upregulating CSF secretion. As such, a cytokine assay was used to evaluate NLRP3-related inflammatory cytokines in the choroid plexus. The choroid plexus assay results indicated that IL-1 β , IL-6, IL-10, TNF- α , and IL-18 were upregulated after ICH-IVH, and MCC950 treatment decreased cytokine levels in the choroid plexus (Fig. 6A). CSF is mainly secreted by the choroid plexus, which could reflect the choroid plexus's function. CSF composition changes have been proven to exist in many kinds of central system diseases. Next, CSF was collected to indicate the cytokine changes. We found that the NLRP3 inflammasome-related cytokines IL-1 β and IL-18 were increased in the CSF (Fig. 6B). Moreover, the NLRP3 inflammasome influences CSF secretion. We tested ion changes in CSF, and we also found Na⁺ and K⁺ increased in CSF after ICH-IVH. When inhibiting NLRP3 activation with MCC950 in the choroid plexus decreased CSF secretion and hydrocephalus, the Na⁺ and K⁺ concentrations also decreased in the CSF (Fig. 6C, D). Based on these results, we explored the transmembrane proteins that alter ion transport and water flow, which could be adjusted by NLRP3.

NKCC1 phosphorylation decreased after ICH-IVH treatment with MCC950 or in *Nlrp3*^{-/-} rats

NKCC1 is the main transporter that contributes to CSF formation by altering Na⁺, K⁺, and Cl⁻ transport across the membrane, and it has been confirmed that NKCC1 phosphorylation (at residues Thr203, Thr207, and Thr212) could influence its function [38]. First, we found that, at 3 days after ICH-IVH, more p-NKCC1-positive cells were found in the ICH-IVH group than in the sham group, and MCC950 treatment decreased the number of p-NKCC1-positive cells in the choroid plexus. After MSU was used to activate NLRP3 again after MCC950 treatment, the number of p-NKCC1-positive cells increased (Fig. 7A, C). Next, for quantitative analyses of NKCC1 phosphorylation levels, western blots were used. Compared with that of the sham group, the protein expression of p-NKCC1 after ICH-IVH was reduced by MCC950, and MSU treatment intervened in this change (Fig. 7B, D). In *Nlrp3*^{-/-} rats, NKCC1 phosphorylation was downregulated compared with that in the control group after ICH-IVH according to p-NKCC1 positive

counting and quantitative analysis (Fig. 7E–H). Based on these results, we presumed that NKCC1 is related to the NLRP3 inflammasome and that NKCC1 is the downstream molecule of NLRP3. The NLRP3/p-NKCC1 pathway activated CSF hypersecretion in the choroid plexus.

Treatment with bumetanide reduced NKCC1 phosphorylation and decreased the CSF secretion rate but did not affect NLRP3 expression

Previous results confirmed that inhibiting NLRP3 using MCC950 or in *Nlrp3*^{-/-} rats decreased p-NKCC1 and improved hydrocephalus. To prove the function of NKCC1 in CSF secretion, NKCC1 could be adjusted by NLRP3. The NKCC1-specific inhibitor bumetanide reduced the number of p-NKCC1-positive cells in the choroid plexus after ICH-IVH (Fig. 8A, B). In addition, bumetanide reduced the CSF secretion rate after ICH-IVH (Fig. 8F, C), and the protein expression of p-NKCC1 was reduced by bumetanide after ICH-IVH (Fig. 8C, D). However, bumetanide treatment did not reduce NLRP3 protein expression in the choroid plexus after ICH-IVH (Fig. 8C, E). Thus, bumetanide could decrease the CSF secretion rate by inhibiting NKCC1 phosphorylation without influencing NLRP3. These results proved that NKCC1 is the downstream molecule of NLRP3.

Reduced inflammatory response in primary choroid plexus epithelial cells treated with MCC950 after LPS or lysis-RBC stimulation

Next, *in vitro* studies were performed to assess the function of NLRP3 on choroid plexus epithelial cells in an inflammatory state. Lipopolysaccharides are endotoxins derived from the outer leaflet of the outer membrane of Gram-negative bacteria that prime the NLRP3 inflammasome in many kinds of cells [39]. Many kinds of blood metabolites, including lysis-RBCs, could induce neuroinflammation after hemorrhage [1, 40]. Therefore, to imitate *in vivo* choroid plexus NLRP3 activation, lysis-RBCs separated from arterial blood were used to treat primary choroid plexus epithelial cells. Primary choroid plexus epithelial control cells were cultured and stimulated with 1 μ g/ml LPS or 1 μ g/ml lysis-RBCs for 12 h, and MCC950 (5 μ M) was used to inhibit NLRP3 inflammasome activation in the lysis-RBC-treated group. NLRP3-positive choroid plexus epithelial cells (marked with AE2: red) were measured in different treatment groups, and LPS and lysis-RBC stimulation activated the NLRP3 inflammasome (Fig. 9A) [41]. Our *in vivo* experimental results showed that p-NKCC1-positive cells were also increased after NLRP3 inflammasome activation. Next, MCC950 treatment decreased NLRP3-positive cells after lysis-RBC treatment, and pNKCC1-positive

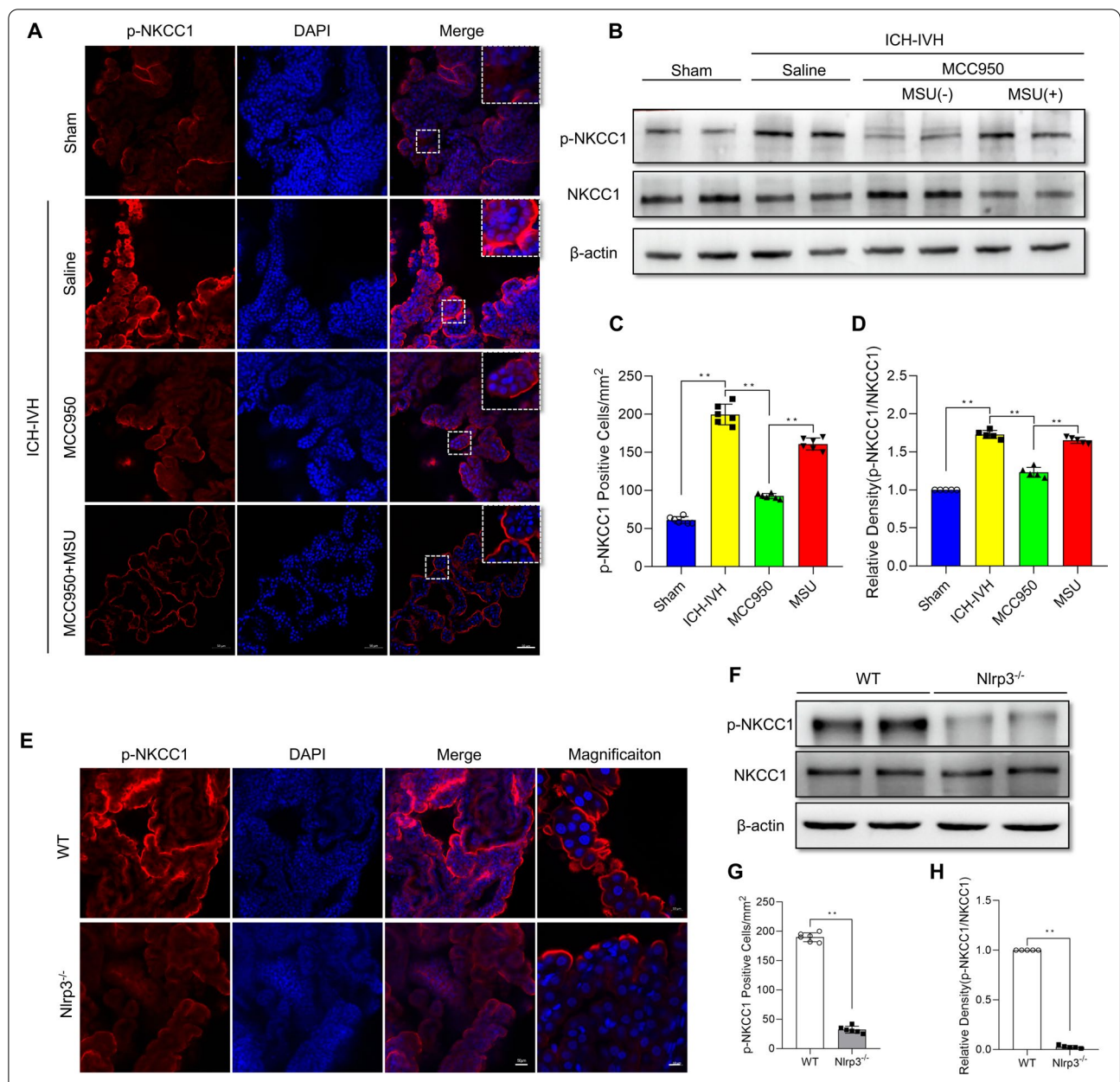
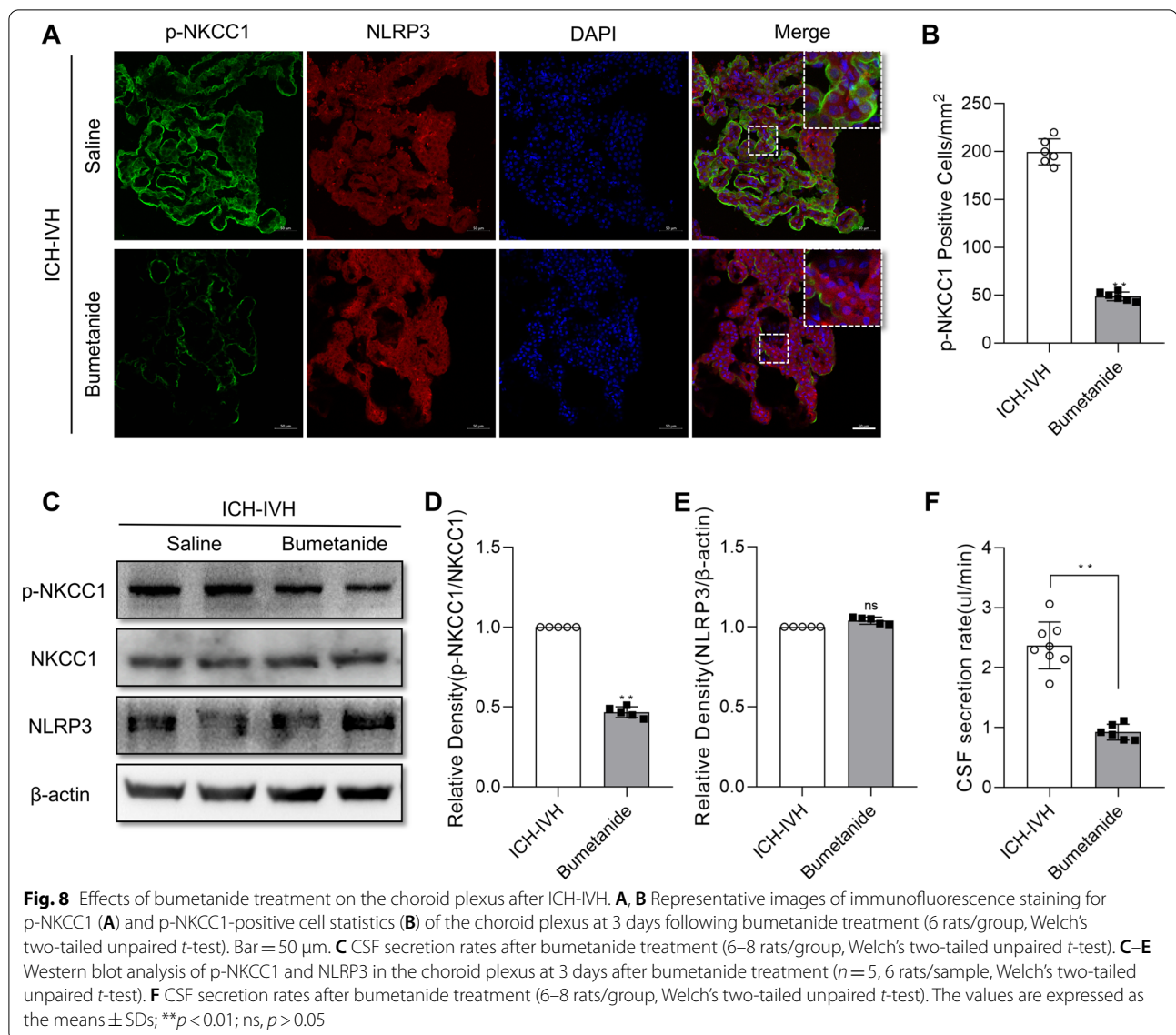


Fig. 7 Effects of MCC950 or Nlrp3 knockout on p-NKCC1 protein levels after ICH-IVH and different treatments. **A, C** Representative images of immunofluorescence staining for p-NKCC1 (**A**) and p-NKCC1-positive cell statistics (**C**) after inhibition of NLRP3 via MCC950 and reactivation with MSU in the choroid plexus on day 3 (6 rats/group, one-way ANOVA). Bar = 50 μm. **B, D** Western blot analysis of p-NKCC1 and NKCC1 in the choroid plexus on day 3 ($n = 5, 6$ rats/group, one-way ANOVA). **E, G** p-NKCC1 staining images of the choroid plexus (**E**) and statistical results of p-NKCC1-positive cell counting (**G**) in control and Nlrp3^{-/-} rats after ICH-IVH (6 rats/group, Welch's two-tailed unpaired t-test). **F, H** Quantitative analysis of p-NKCC1 and NKCC1 levels in the choroid plexus in control and Nlrp3^{-/-} rats after ICH-IVH ($n = 5, 6$ rats/group, Welch's two-tailed unpaired t-test). **C, D** ICH-IVH indicates ICH-IVH (WT) + saline; MCC950 indicates ICH-IVH (WT) + MCC950; MSU indicates ICH-IVH (WT) + MCC950 + MSU. The values are expressed as the means ± SDs; ** $p < 0.01$; * $p < 0.05$

cells also decreased (Fig. 9B). Furthermore, western blots were used to quantitatively analyze NLRP3 and p-NKCC1 levels in primary choroid plexus epithelial cells (ChP), which showed results similar to those shown before (Fig. 9C–E). In total, the NLRP3/

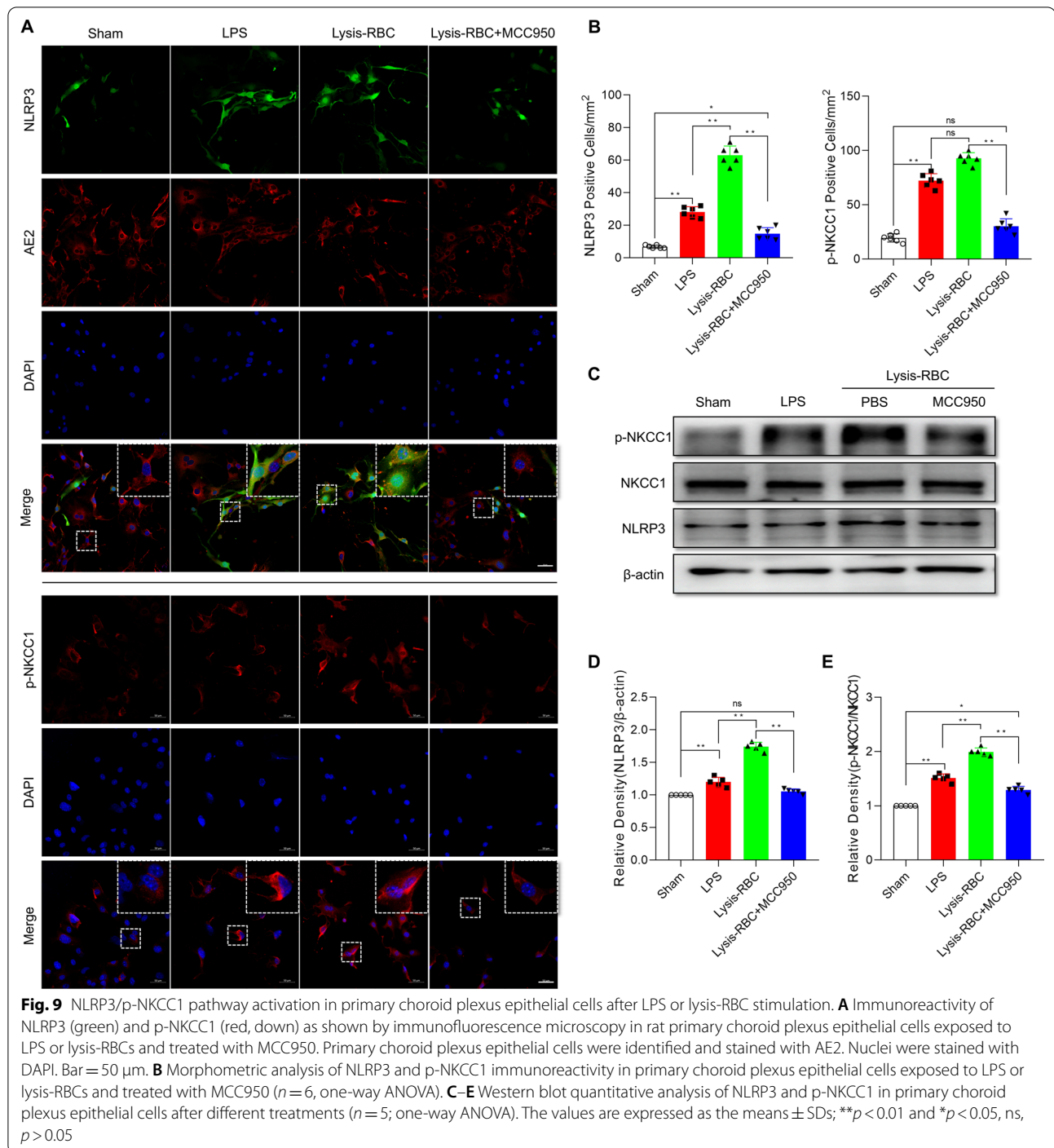
pNKCC1 pathway was activated in ChP after LPS or lysis-RBC stimulation, and MCC950 treatment reduced the activity of the NLRP3/pNKCC1 pathway.



Na⁺ and K⁺ efflux driving H₂O outflow after the NLRP3/pNKCC1 pathway is activated in primary choroid plexus epithelial cells

As reported, NKCC1 is an important transporter located in primary epithelial cells. NKCC1 alters transmembrane ion flow, including Na⁺, K⁺, and Cl⁻, and H₂O transport across the membrane. Therefore, Na⁺ and K⁺ concentration changes could be used to reflect transmembrane water transport [42]. The CSF detection results proved that Na⁺ and K⁺ increased after hemorrhage, and inhibiting NLRP3 via MCC950 decreased Na⁺ and K⁺ concentrations in CSF. First, we evaluated Na⁺ and K⁺ concentration. SBFI and PBF1 were used to measure Na⁺ and K⁺ concentrations in ChP. According to SBFI and PBF1 staining images and statistical results, we found

that after activation of the NLRP3/pNKCC1 pathway via LPS or lysis-RBCs, the Na⁺ and K⁺ ion concentrations in cells decreased, and using MCC950 to inhibit NLRP3 intervened in the transport of ions across the membrane (Fig. 10A–C). Next, for SBFI- and PBF1-loaded ChP, we monitored Na⁺ and K⁺ dynamics for 300 s when LPS and lysis-RBCs were added to the media. Intracellular Na⁺ and K⁺ decreased immediately after stimulators were added compared with that in the sham group, and the addition of MCC950 weakened ion and water outflow (Fig. 10D, E). Then, we measured Na⁺ and K⁺ in the media for reevaluation via ICP-OES and found that the Na⁺ and K⁺ concentrations in the media were elevated in both the LPS- and lysis-RBC-treated groups, and inhibiting NLRP3/pNKCC1 decreased the ion concentration in



(See figure on next page.)

Fig. 10 NKCC1-mediated transmembrane cotransport of ions and water after NLRP3 activation. **A** Representative images of Na⁺ (SBFI) and K⁺ (PBFI) after LPS or lysis-RBC exposure and MCC950 treatment in primary choroid plexus epithelial cells. Bar = 50 μm. **B** Statistical results of Na⁺ concentrations in primary choroid plexus epithelial cells according to SBFI staining ($n=6$, one-way ANOVA). **C** Statistical results of K⁺ concentrations in primary choroid plexus epithelial cells according to PBFI staining ($n=6$, one-way ANOVA). **D** Time course of Na⁺ concentration changes in primary choroid plexus epithelial cells after the addition of stimulators and MCC950 treatment ($n=6$). **E** Changes in intracellular K⁺ concentrations over time after different treatments ($n=6$). **F–G** Na⁺ and K⁺ concentrations measured by ICP-OES in culture media after LPS and lysis-RBC stimulation and MCC950 treatment ($n=6$, one-way ANOVA). The values are expressed as the means \pm SDs; ** $p < 0.01$ and * $p < 0.05$

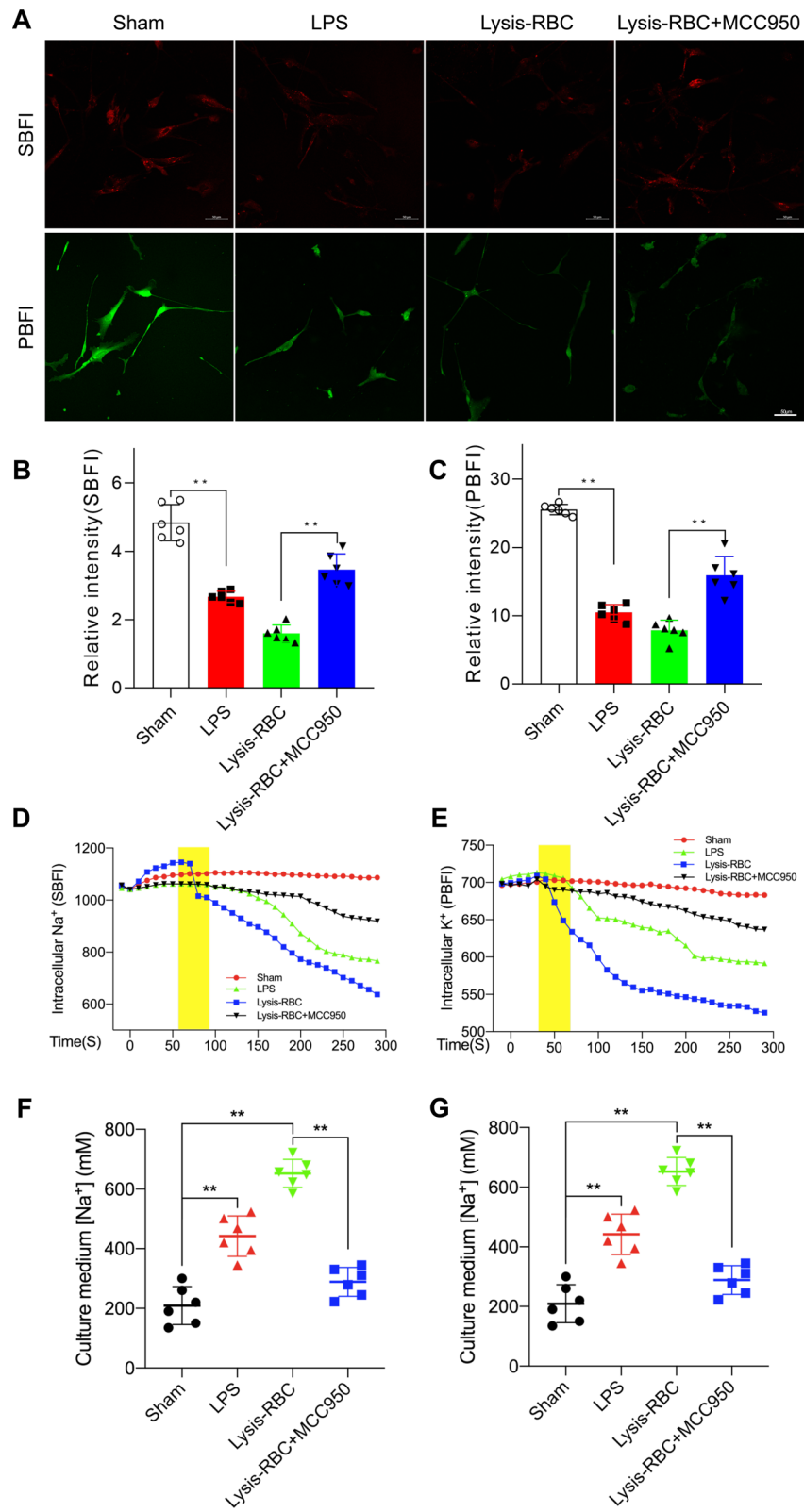


Fig. 10 (See legend on previous page.)

the medium (Fig. 10F, G). In summary, NLRP3/p-NKCC1 induced the outflow of water from choroid plexus epithelial cells.

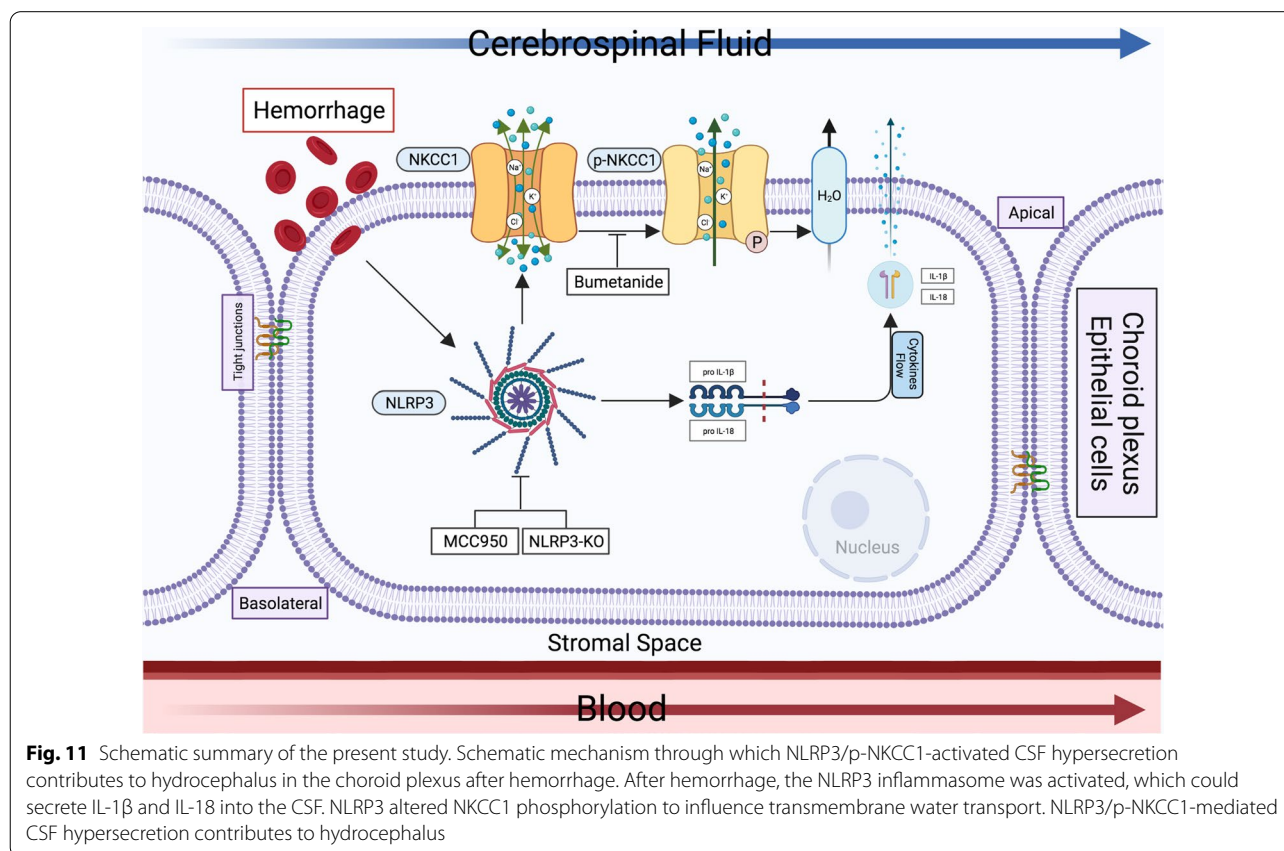
Discussion

We demonstrated that activation of the NLRP3 inflammasome contributed to hydrocephalus by mediating CSF hypersecretion in the choroid plexus after ICH-IVH. Furthermore, the NLRP3 inflammasome influenced CSF secretion by controlling NKCC1 phosphorylation in the choroid plexus, and NKCC1 affected hydrocephalus by transporting ions across the membrane together with water. Combined, these results suggest that the NLRP3 inflammasome contributes to the pathogenesis of hydrocephalus after ICH-IVH (Fig. 11).

Hydrocephalus is a severe complication after ICH, especially with ventricular extension [43, 44]. Most studies on hydrocephalus after hemorrhage have been based on the IVH model and have not been able to simulate the clinical pathogenesis of hydrocephalus after hemorrhage in infants or adults [45]. As revealed by our previous study, hydrocephalus and brain tissue injury were found to be more serious in a rat model of ICH-IVH than in an IVH model, which thus conforms more closely to the results of a clinical model [9]. Therefore, we used the

ICH-IVH model to explore the pathogenesis of hydrocephalus in this study.

It is a commonly held view that hydrocephalus after hemorrhage is caused by abnormalities in the CSF drainage pathway, particularly related to the cerebral aqueduct, fourth ventricular outlets, ependymal epithelium damage, arachnoid villi or granulations or choroid plexus inflammation. Few animal studies have investigated the cerebral aqueduct or the outlets of the fourth ventricle. Arachnoid granulations are considered sites of absorption. The presence and morphology of arachnoid granulations are different between humans and animals [46]. However, arachnoid granulations are not completely developed in infants with hydrocephalus [47, 48]. Nerve tissue with lymphatic vessels has been widely reported [49–51]. It is accepted that a considerable amount of CSF flows into lymphatic vessels and that lymphatic outflow may result in hydrocephalus [52]. Ependymal cilium beating generates flow of the CSF within the brain cavities and aids in maintaining the patency of the ventricular system [53, 54]. Clinical and preclinical data suggest that the loss of developing and mature ciliated epithelial cells contributes to the development of hydrocephalus after hemorrhage [55–57]. All these studies focused on the outflow dysfunction of CSF. The choroid plexus is located



at the base of each of the four ventricles. Regarding the production of CSF in the choroid plexus, few relevant studies have been conducted. Nuclear factor κ B (NF- κ B) signaling is activated by CSF barrier cells of the choroid plexus and ependymal lining after IVH [58]. Moreover, systemic inflammation stimulates TLRs in the choroid plexus, which may lead to disturbances in choroid plexus barrier function [59]. A recent study proved that TLR4-dependent inflammation leading to CSF hypersecretion plays a role in the development of hydrocephalus after hemorrhage [11]. It has been reported that NLRP3 mediates many kinds of nervous system injuries after ICH, subarachnoid hemorrhage or traumatic brain injury [22, 60], but there are no studies about the NLRP3 inflammasome in hydrocephalus. In addition, transcriptome and proteomics analyses of the choroid plexus proved that the inflammatory response, including NLRP3 inflammasome activation, was activated. It has also been proven through single-cell RNA-seq that the NLRP3 inflammasome is expressed in epithelial cells. Based on these findings, we investigated the characteristics of the NLRP3 inflammasome and the choroid plexus and proved that NLRP3 contributes to hydrocephalus by increasing CSF secretion in the choroid plexus. Current CSF secretion methods indirect for measuring CSF formation in vivo include tracer dilution, MRI and others. CSF formation was measured using the indirect tracer dilution method with blue dextran, but the limitation cannot be synchronized with pharmacological manipulations [61]. A single method was used in this study to measure CSF secretion, but other approaches should also be explored. Furthermore, blood components are complex, which makes identifying the specific components that activate the NLRP3 inflammasome in the choroid plexus unclear. Many factors, such as iron, hemoglobin and transforming growth factor- β 1, contribute to hydrocephalus after hemorrhage [9, 62, 63]. In *in vitro* studies, only lysis-RBCs were used to stimulate primary choroid plexus epithelial cells, which activated the NLRP3 inflammasome. In future studies, we aim to explore what activates the NLRP3 inflammasome after ICH-IVH in the choroid plexus.

After we discovered that the NLRP3 inflammasome became activated after ICH-IVH in the choroid plexus, we attempted to elucidate the molecular mechanisms occurring between the NLRP3 inflammasome and CSF formation. Approximately 500 ml of fluid is produced by the choroid plexus in the mammalian brain. CSF production is assumed to take place by the transport of osmotically active ions, the passive movement of water and the water channel aquaporin. NKCC1, K^+/Cl^- cotransporters (KCCs), Na^+ -coupled bicarbonate transporters, and Na^+/K^+ -ATPase are the main ion transporters that adapt

to the formation of CSF, and NKCC1 plays an important role among these transporters [13, 14, 64–68]. However, CSF production decreased by only 20% in AQP1 knock-out mice [69]. AQP4 also contributes to CSF formation, but its function is also limited [70]. NKCC1 is located at the luminal membrane and indicates its unique outward transport direction, which mediates the cotransport of water by ion transport across the membrane in an inflammatory state. Among the concentrations of Na^+ , K^+ , and Cl^- altered by NKCC1, we detected Na^+ and K^+ concentrations in primary choroid plexus epithelial cells. The main regulatory molecule NKCC1 was selected in this study, and it was briefly proven that NKCC1 is a molecular component in NLRP3-mediated CSF hypersecretion. Interestingly, the ion concentration results confirmed our previous results; however, Na^+ and K^+ showed different change trends, and the degree of Na^+ outflow was more severe than that of K^+ outflow. K^+ efflux and inflammation stimulators (LPS or lysis-RBC) can activate the NLRP3 inflammasome [71, 72]. After the NLRP3/p-NKCC1 pathway is activated by stimulators in the choroid plexus, p-NKCC1 mediates Na^+ and K^+ outflow, and K^+ efflux activates the NLRP3 inflammasome, which results in a positive feedback cascade amplification effect. Due to the limited evidence, further studies are still needed to clarify the mechanism of NLRP3-mediated CSF hypersecretion after ICH-IVH.

In this study, we observed that ICH-IVH induced CSF hypersecretion by activating the NLRP3 inflammasome, and the ion cotransporter NKCC1 regulating CSF secretion also participated in this process. In addition, we found blood–CSF barrier disruption and lipid droplet (LD) formation in the choroid plexus by accident.

The most widely recognized role of the choroid plexus is in the formation of the blood–CSF barrier, whereby it serves as a controller of the internal CNS microenvironment [73]. Blood–CSF barrier integrity is impaired in the pathology of many common CNS disorders, such as Alzheimer's disease, Parkinson's disease and stroke [74]. Neuroinflammation is a natural response to CNS injury and disease during blood–CSF barrier dysfunction [75]. We found that after blood–CSF barrier dysfunction due to ICH-IVH, inhibition of the NLRP3 inflammasome could improve the integrity of the blood–CSF barrier. Nonetheless, the relationship between the integrity of the blood–CSF barrier and the NLRP3 inflammasome requires further exploration. LDs are major lipid storage organelles of eukaryotic cells and are central players in anti-infection processes [76]. Further studies will focus on what components in the blood contribute to NLRP3 inflammasome activation, blood–CSF barrier disruption and LD formation and the relationship between them and hydrocephalus. Although we identified a new therapeutic

target for hydrocephalus after hemorrhage, the pathogenesis of hydrocephalus requires further exploration for a complete understanding.

Conclusion

Our results showed that activation of NLRP3 in the choroid plexus contributed to increased CSF secretion and aggravated hydrocephalus after ICH-IVH, and NLRP3 impacted CSF secretion by regulating the NKCC1 phosphorylation level. In addition, NKCC1 phosphorylation mediated more coupling of ion (Na^+ and K^+) efflux to transmembrane water transport in primary choroid plexus epithelial cells after ICH-IVH, which also contributed to aggravated hydrocephalus. This study provides evidence that inhibiting NLRP3 may be a potential therapeutic approach for preventing hydrocephalus after ICH-IVH.

Abbreviations

ICH: Intracerebral hemorrhage; CSF: Cerebrospinal fluid; TLR4: Toll-like receptor 4; NKCC1: $\text{Na}^+/\text{K}^+/\text{2Cl}^-$ cotransporter; ICH-IVH: Intracerebral hemorrhage with ventricular extension; ARRIVE: Animal Research: Reporting of In Vivo Experiments; mNSS: Modified Neurological Severity Score; FPKM: Fragments per kilobase per million; IVH: Intraventricular hemorrhage; MRI: Magnetic resonance imaging; ChP: Primary choroid plexus epithelial cells.

Supplementary Information

The online version contains supplementary material available at <https://doi.org/10.1186/s12974-022-02530-x>.

Additional file 1. Statistical Results in Figures.

Acknowledgements

Not applicable.

Authors' contributions

YC and HF conceived and designed the study. ZZ, QT, PG, SH, ZJ and XL acquired and analyzed the data. ZZ and YC drafted a substantial portion of the manuscript and revised the manuscript. All authors read and approved the present version of the manuscript to be published.

Funding

This work was supported by State Key Laboratory of Trauma, Burn and Combined Injury (SKLYQ202002 to Yujie Chen), National Natural Science Foundation of China (82030036 to Hua Feng), Chongqing Talent Program (4139Z2391 to Hua Feng) and Southwest Hospital (SWH2018BJKJ-05 to Yujie Chen).

Availability of data and materials

All data generated or analyzed during this study are included in this published article. The datasets used and/or analyzed during the current study are available from the corresponding author on reasonable request.

Declarations

Ethics approval and consent to participate

All experiments are reported in compliance with the Animal Research: Reporting in vivo Experiments (ARRIVE) guidelines. The experimental protocols were approved by the Laboratory Animal Welfare and Ethics Committee of Third Military Medical University (AMUWEC2020762) and performed according to the Guide for the Care and Use of Laboratory Animals.

Consent for publication

Not applicable.

Competing interests

The authors declare that they have no competing interests.

Author details

¹Department of Neurosurgery and State Key Laboratory of Trauma, Burn and Combined Injury, Southwest Hospital, Third Military Medical University (Army Medical University), 29 Gaotanyan Street, Shapingba District, Chongqing 400038, China. ²Chongqing Key Laboratory of Precision Neuromedicine and Neuroregeneration, Southwest Hospital, Third Military Medical University (Army Medical University), Chongqing 400038, China. ³Chongqing Clinical Research Center for Neurosurgery, Southwest Hospital, Third Military Medical University (Army Medical University), Chongqing 400038, China. ⁴CAS Key Laboratory of Separation Science for Analytical Chemistry, Dalian Institute of Chemical Physics, Chinese Academy of Sciences, Dalian 116023, China.

Received: 22 October 2021 Accepted: 14 June 2022

Published online: 21 June 2022

References

- Keep RF, Hua Y, Xi G. Intracerebral haemorrhage: mechanisms of injury and therapeutic targets. *Lancet Neurol.* 2012;11(8):720–31.
- Mustanoja S, Satopaa J, Meretoja A, Putaala J, Strbian D, Curtze S, et al. Extent of secondary intraventricular hemorrhage is an independent predictor of outcomes in intracerebral hemorrhage: data from the Helsinki ICH Study. *Int J Stroke.* 2015;10(4):576–81.
- Halleivi H, Albright KC, Aronowski J, Barreto AD, Martin-Schild S, Khaja AM, et al. Intraventricular hemorrhage: anatomic relationships and clinical implications. *Neurology.* 2008;70(11):848–52.
- Hu R, Zhang C, Xia J, Ge H, Zhong J, Fang X, et al. Long-term outcomes and risk factors related to hydrocephalus after intracerebral hemorrhage. *Transl Stroke Res.* 2020;12:31–8.
- Dmello D, Cruz-Flores S, Matuschak GM. Moderate hypothermia with intracranial pressure monitoring as a therapeutic paradigm for the management of acute liver failure: a systematic review. *Intensive Care Med.* 2010;36(2):210–3.
- Kahle KT, Kulkarni AV, Limbrick DD Jr, Warf BC. Hydrocephalus in children. *Lancet.* 2016;387(10020):788–99.
- Santucci JA, Ross SR, Greenert JC, Aghaei F, Ford L, Hollabaugh KM, et al. Radiological estimation of intracranial blood volume and occurrence of hydrocephalus determines stress-induced hyperglycemia after aneurysmal subarachnoid hemorrhage. *Transl Stroke Res.* 2018;10:327.
- McAllister JP 2nd, Williams MA, Walker ML, Kestle JR, Relkin NR, Anderson AM, et al. An update on research priorities in hydrocephalus: overview of the third National Institutes of Health-sponsored symposium "Opportunities for Hydrocephalus Research: Pathways to Better Outcomes." *J Neurosurg.* 2015;123(6):1427–38.
- Chen Q, Tang J, Tan L, Guo J, Tao Y, Li L, et al. Intracerebral hematoma contributes to hydrocephalus after intraventricular hemorrhage via aggravating iron accumulation. *Stroke.* 2015;46(10):2902–8.
- Mondejar V, Patsalides A. The role of arachnoid granulations and the glymphatic system in the pathophysiology of idiopathic intracranial hypertension. *Curr Neurol Neurosci Rep.* 2020;20(7):20.
- Karim JK, Zhang J, Kurland DB, Theriault BC, Duran D, Stokum JA, et al. Inflammation-dependent cerebrospinal fluid hypersecretion by the choroid plexus epithelium in posthemorrhagic hydrocephalus. *Nat Med.* 2017;23(8):997–1003.
- Hallaert GG, Vanhauwaert DJ, Logghe K, Van den Broecke C, Baert E, Van Roost D, et al. Endoscopic coagulation of choroid plexus hyperplasia. *J Neurosurg Pediatr.* 2012;9(2):169–77.
- Spector R, Keep RF, Robert Snodgrass S, Smith QR, Johanson CE. A balanced view of choroid plexus structure and function: focus on adult humans. *Exp Neurol.* 2015;267:78–86.
- Steffensen AB, Oernbo EK, Stoica A, Gerkau NJ, Barbuskaite D, Tritsarlis K, et al. Cotransporter-mediated water transport underlying cerebrospinal fluid formation. *Nat Commun.* 2018;9(1):2167.

15. Choe S, Rosenberg JM, Abramson J, Wright EM, Grabe M. Water permeation through the sodium-dependent galactose cotransporter vSGLT. *Biophys J*. 2010;99(7):L56–8.
16. Skorput AG, Lee SM, Yeh PW, Yeh HH. The NKCC1 antagonist bumetanide mitigates interneuronopathy associated with ethanol exposure in utero. *Elife*. 2019;8.
17. Hoffman HM, Broderick L. The role of the inflammasome in patients with autoinflammatory diseases. *J Allergy Clin Immunol*. 2016;138(1):3–14.
18. Yang SJ, Shao GF, Chen JL, Gong J. The NLRP3 inflammasome: an important driver of neuroinflammation in hemorrhagic stroke. *Cell Mol Neurobiol*. 2018;38(3):595–603.
19. Heneka MT, McManus RM, Latz E. Inflammasome signalling in brain function and neurodegenerative disease. *Nat Rev Neurosci*. 2018;19(10):610–21.
20. Gros Lambert M, Py BF. Spotlight on the NLRP3 inflammasome pathway. *J Inflamm Res*. 2018;11:359–74.
21. Cheng S, Gao W, Xu X, Fan H, Wu Y, Li F, et al. Methylprednisolone sodium succinate reduces BBB disruption and inflammation in a model mouse of intracranial haemorrhage. *Brain Res Bull*. 2016;127:226–33.
22. Ren H, Kong Y, Liu Z, Zang D, Yang X, Wood K, et al. Selective NLRP3 (pyrin domain-containing protein 3) inflammasome inhibitor reduces brain injury after intracerebral hemorrhage. *Stroke*. 2018;49(1):184–92.
23. Zeng J, Chen Y, Ding R, Feng L, Fu Z, Yang S, et al. Isoliquiritigenin alleviates early brain injury after experimental intracerebral hemorrhage via suppressing ROS- and/or NF- κ B-mediated NLRP3 inflammasome activation by promoting Nrf2 antioxidant pathway. *J Neuroinflammation*. 2017;14(1):119.
24. Chen Q, Zhang J, Guo J, Tang J, Tao Y, Li L, et al. Chronic hydrocephalus and perihematomal tissue injury developed in a rat model of intracerebral hemorrhage with ventricular extension. *Transl Stroke Res*. 2015;6(2):125–32.
25. Chen J, Sanberg PR, Li Y, Wang L, Lu M, Willing AE, et al. Intravenous administration of human umbilical cord blood reduces behavioral deficits after stroke in rats. *Stroke*. 2001;32(11):2682–8.
26. Pang J, Peng J, Matei N, Yang P, Kuai L, Wu Y, et al. Apolipoprotein E exerts a whole-brain protective property by promoting M1 ϕ Microglia quiescence after experimental subarachnoid hemorrhage in mice. *Transl Stroke Res*. 2018;9(6):654–68.
27. Bonetto A, Andersson DC, Waning DL. Assessment of muscle mass and strength in mice. *Bonekey Rep*. 2015;4:732.
28. Karimy JK, Kahle KT, Kurland DB, Yu E, Gerzanich V, Simard JM. A novel method to study cerebrospinal fluid dynamics in rats. *J Neurosci Methods*. 2015;241:78–84.
29. Xi G, Keep RF, Hua Y, Xiang J, Hoff JT. Attenuation of thrombin-induced brain edema by cerebral thrombin preconditioning. *Stroke*. 1999;30(6):1247–55.
30. Ma Q, Huang B, Khatibi N, Rolland W 2nd, Suzuki H, Zhang JH, et al. PDGFR- α inhibition preserves blood–brain barrier after intracerebral hemorrhage. *Ann Neurol*. 2011;70(6):920–31.
31. Jusue-Torres I, Jeon LH, Sankey EW, Lu J, Vivas-Buitrago T, Crawford JA, et al. A novel experimental animal model of adult chronic hydrocephalus. *Neurosurgery*. 2016;79(5):746–56.
32. Okauchi M, Hua Y, Keep RF, Morgenstern LB, Xi G. Effects of deferoxamine on intracerebral hemorrhage-induced brain injury in aged rats. *Stroke*. 2009;40(5):1858–63.
33. MacLellan CL, Silasi G, Poon CC, Edmundson CL, Buist R, Peeling J, et al. Intracerebral hemorrhage models in rat: comparing collagenase to blood infusion. *J Cereb Blood Flow Metab*. 2008;28(3):516–25.
34. Shiroguchi K, Jia TZ, Sims PA, Xie XS. Digital RNA sequencing minimizes sequence-dependent bias and amplification noise with optimized single-molecule barcodes. *Proc Natl Acad Sci USA*. 2012;109(4):1347–52.
35. Wisniewski JR, Zougman A, Nagaraj N, Mann M. Universal sample preparation method for proteome analysis. *Nat Methods*. 2009;6(5):359–62.
36. Lallai V, Ahmed A, Fowler CD. Method for primary epithelial cell culture from the rat choroid plexus. *Bio Protoc*. 2020;10(4):e3532.
37. MacAulay N. Molecular mechanisms of brain water transport. *Nat Rev Neurosci*. 2021;22(6):326–44.
38. Vitari AC, Thastrup J, Rafiqi FH, Deak M, Morrice NA, Karlsson HK, et al. Functional interactions of the SPAK/OSR1 kinases with their upstream activator WNK1 and downstream substrate NKCC1. *Biochem J*. 2006;397(1):223–31.
39. Venegas C, Kumar S, Franklin BS, Dierkes T, Brinkschulte R, Tejera D, et al. Microglia-derived ASC specks cross-seed amyloid-beta in Alzheimer's disease. *Nature*. 2017;552(7685):355–61.
40. Wilkinson DA, Pandey AS, Thompson BG, Keep RF, Hua Y, Xi G. Injury mechanisms in acute intracerebral hemorrhage. *Neuropharmacology*. 2018;134(Pt B):240–8.
41. Zhu L, Stein LR, Kim D, Ho K, Yu GQ, Zhan L, et al. Klotho controls the brain-immune system interface in the choroid plexus. *Proc Natl Acad Sci USA*. 2018;115(48):E11388–96.
42. Koumangoye R, Bastarache L, Delpire E. NKCC1: newly found as a human disease-causing ion transporter. *Function (Oxf)*. 2021;2(1):zqaa028.
43. Balamji JS, Buchan AM. Complications of intracerebral haemorrhage. *Lancet Neurol*. 2012;11(1):101–18.
44. Strahle J, Garton HJ, Maher CO, Muraszko KM, Keep RF, Xi G. Mechanisms of hydrocephalus after neonatal and adult intraventricular hemorrhage. *Transl Stroke Res*. 2012;3(Suppl 1):25–38.
45. Schlunk F, Greenberg SM. The pathophysiology of intracerebral hemorrhage formation and expansion. *Transl Stroke Res*. 2015;6(4):257–63.
46. Mann JD, Butler AB, Rosenthal JE, Maffeo CJ, Johnson RN, Bass NH. Regulation of intracranial pressure in rat, dog, and man. *Ann Neurol*. 1978;3(2):156–65.
47. Mack J, Squier W, Eastman JT. Anatomy and development of the meninges: implications for subdural collections and CSF circulation. *Pediatr Radiol*. 2009;39(3):200–10.
48. Oi S, Di Rocco C. Proposal of “evolution theory in cerebrospinal fluid dynamics” and minor pathway hydrocephalus in developing immature brain. *Childs Nerv Syst*. 2006;22(7):662–9.
49. Johnston M, Zakharov A, Papaiconomou C, Salmasi G, Armstrong D. Evidence of connections between cerebrospinal fluid and nasal lymphatic vessels in humans, non-human primates and other mammalian species. *Cerebrospinal Fluid Res*. 2004;1(1):2.
50. Ludemann W, Berens von Rautenfeld D, Samii M, Brinker T. Ultrastructure of the cerebrospinal fluid outflow along the optic nerve into the lymphatic system. *Childs Nerv Syst*. 2005;21(2):96–103.
51. Zakharov A, Papaiconomou C, Koh L, Djenic J, Bozanovic-Sosic R, Johnston M. Integrating the roles of extracranial lymphatics and intracranial veins in cerebrospinal fluid absorption in sheep. *Microvasc Res*. 2004;67(1):96–104.
52. Nagra G, Li J, McAllister JP 2nd, Miller J, Wagshul M, Johnston M. Impaired lymphatic cerebrospinal fluid absorption in a rat model of kaolin-induced communicating hydrocephalus. *Am J Physiol Regul Integr Comp Physiol*. 2008;294(5):R1752–9.
53. Ibanez-Tallon I, Gorokhova S, Heintz N. Loss of function of axonemal dynein Mdnah5 causes primary ciliary dyskinesia and hydrocephalus. *Hum Mol Genet*. 2002;11(6):715–21.
54. Ibanez-Tallon I, Pagenstecher A, Fliegau M, Olbrich H, Kispert A, Ketelsen UP, et al. Dysfunction of axonemal dynein heavy chain Mdnah5 inhibits ependymal flow and reveals a novel mechanism for hydrocephalus formation. *Hum Mol Genet*. 2004;13(18):2133–41.
55. Wallmeier J, Nielsen KG, Kuehni CE, Lucas JS, Leigh MW, Zariwala MA, et al. Motile ciliopathies. *Nat Rev Dis Primers*. 2020;6(1):77.
56. Castaneyra-Ruiz L, Morales DM, McAllister JP, Brody SL, Isaacs AM, Strahle JM, et al. Blood exposure causes ventricular zone disruption and glial activation in vitro. *J Neuropathol Exp Neurol*. 2018;77(9):803–13.
57. McAllister JP, Guerra MM, Ruiz LC, Jimenez AJ, Dominguez-Pinos D, Sival D, et al. Ventricular zone disruption in human neonates with intraventricular hemorrhage. *J Neuropathol Exp Neurol*. 2017;76(5):358–75.
58. Simard PF, Tosun C, Melnichenko L, Ivanova S, Gerzanich V, Simard JM. Inflammation of the choroid plexus and ependymal layer of the ventricle following intraventricular hemorrhage. *Transl Stroke Res*. 2011;2(2):227–31.
59. Stridl L, Ek CJ, Wang X, Nilsson H, Mallard C. Regulation of Toll-like receptors in the choroid plexus in the immature brain after systemic inflammatory stimuli. *Transl Stroke Res*. 2013;4(2):220–7.
60. Kuwar R, Rolfe A, Di L, Xu H, He L, Jiang Y, et al. A novel small molecular NLRP3 inflammasome inhibitor alleviates neuroinflammatory response following traumatic brain injury. *J Neuroinflamm*. 2019;16(1):81.
61. Chiu C, Miller MC, Caralopoulos IN, Worden MS, Brinker T, Gordon ZN, et al. Temporal course of cerebrospinal fluid dynamics and amyloid accumulation in the aging rat brain from three to thirty months. *Fluids Barriers CNS*. 2012;9(1):3.

62. Gao C, Du H, Hua Y, Keep RF, Strahle J, Xi G. Role of red blood cell lysis and iron in hydrocephalus after intraventricular hemorrhage. *J Cereb Blood Flow Metab.* 2014;34(6):1070–5.
63. Cherian S, Thoresen M, Silver IA, Whitelaw A, Love S. Transforming growth factor-beta_s in a rat model of neonatal posthaemorrhagic hydrocephalus. *Neuropathol Appl Neurobiol.* 2004;30(6):585–600.
64. Hamann S, Herrera-Perez JJ, Zeuthen T, Alvarez-Leefmans FJ. Cotransport of water by the Na⁺-K⁺-2Cl⁻ cotransporter NKCC1 in mammalian epithelial cells. *J Physiol.* 2010;588(Pt 21):4089–101.
65. Zeuthen T. Cotransport of K⁺, Cl⁻ and H₂O by membrane proteins from choroid plexus epithelium of *Necturus maculosus*. *J Physiol.* 1994;478(Pt 2):203–19.
66. Damkier HH, Brown PD, Praetorius J. Cerebrospinal fluid secretion by the choroid plexus. *Physiol Rev.* 2013;93(4):1847–92.
67. Hladky SB, Barrand MA. Fluid and ion transfer across the blood–brain and blood–cerebrospinal fluid barriers; a comparative account of mechanisms and roles. *Fluids Barriers CNS.* 2016;13(1):19.
68. Praetorius J, Damkier HH. Transport across the choroid plexus epithelium. *Am J Physiol Cell Physiol.* 2017;312(6):C673–86.
69. Oshio K, Watanabe H, Song Y, Verkman AS, Manley GT. Reduced cerebrospinal fluid production and intracranial pressure in mice lacking choroid plexus water channel Aquaporin-1. *FASEB J.* 2005;19(1):76–8.
70. Hasan-Olive MM, Enger R, Hansson HA, Nagelhus EA, Eide PK. Loss of perivascular aquaporin-4 in idiopathic normal pressure hydrocephalus. *Glia.* 2019;67(1):91–100.
71. Gross CJ, Mishra R, Schneider KS, Medard G, Wettmarshausen J, Dittlein DC, et al. K(+) efflux-independent NLRP3 inflammasome activation by small molecules targeting mitochondria. *Immunity.* 2016;45(4):761–73.
72. Munoz-Planillo R, Kuffa P, Martinez-Colon G, Smith BL, Rajendiran TM, Nunez G. K(+) efflux is the common trigger of NLRP3 inflammasome activation by bacterial toxins and particulate matter. *Immunity.* 2013;38(6):1142–53.
73. Liddelow SA. Development of the choroid plexus and blood-CSF barrier. *Front Neurosci.* 2015;9:32.
74. Neuwelt EA, Bauer B, Fahlke C, Fricker G, Iadecola C, Janigro D, et al. Engaging neuroscience to advance translational research in brain barrier biology. *Nat Rev Neurosci.* 2011;12(3):169–82.
75. Daneman R, Zhou L, Kebede AA, Barres BA. Pericytes are required for blood–brain barrier integrity during embryogenesis. *Nature.* 2010;468(7323):562–6.
76. Bosch M, Sanchez-Alvarez M, Fajardo A, Kapetanovic R, Steiner B, Dutra F, et al. Mammalian lipid droplets are innate immune hubs integrating cell metabolism and host defense. *Science.* 2020;370(6514):eaay8085.

Publisher's Note

Springer Nature remains neutral with regard to jurisdictional claims in published maps and institutional affiliations.

Ready to submit your research? Choose BMC and benefit from:

- fast, convenient online submission
- thorough peer review by experienced researchers in your field
- rapid publication on acceptance
- support for research data, including large and complex data types
- gold Open Access which fosters wider collaboration and increased citations
- maximum visibility for your research: over 100M website views per year

At BMC, research is always in progress.

Learn more biomedcentral.com/submissions

